Taylor & Francis
Taylor & Francis Group

REPORT

🔓 OPEN ACCESS ✓ Check for updates

Development of a high yielding expression platform for the introduction of non-natural amino acids in protein sequences

Gargi Roy [a], Jason Reier [b], Andrew Garcia[a], Tom Martin [a], Megan Rice[a], Jihong Wang [c*], Meagan Prophet [c], Ronald Christie[a], William Dall'Acqua[a], Sanjeev Ahuja [b], Michael A Bowen[a**], and Marcello Marelli [a]

aAntibody Discovery and Protein Engineering, AstraZeneca, Gaithersburg, Maryland, USA; bCell Culture and Fermentation Sciences, AstraZeneca, Gaithersburg, Maryland, USA; cAnalytical Sciences, AstraZeneca, Gaithersburg, Maryland, USA

ABSTRACT

The ability to genetically encode non-natural amino acids (nnAAs) into proteins offers an expanded tool set for protein engineering. nnAAs containing unique functional moieties have enabled the study of post-translational modifications, protein interactions, and protein folding. In addition, nnAAs have been developed that enable a variety of biorthogonal conjugation chemistries that allow precise and efficient protein conjugations. These are being studied to create the next generation of antibody-drug conjugates with improved efficacy, potency, and stability for the treatment of cancer. However, the efficiency of nnAA incorporation, and the productive yields of cell-based expression systems, have limited the utility and widespread use of this technology. We developed a process to isolate stable cell lines expressing a pyrrolysyl-tRNA synthetase/tRNApyl pair capable of efficient nnAA incorporation. Two different platform cell lines generated by these methods were used to produce IgG-expressing cell lines with normalized antibody titers of 3 g/L using continuous perfusion. We show that the antibodies produced by these platform cells contain the nnAA functionality that enables facile conjugations. Characterization of these highly active and robust platform hosts identified key parameters that affect nnAA incorporation efficiency. These highly efficient host platforms may help overcome the expression challenges that have impeded the developability of this technology for manufacturing proteins with nnAAs and represents an important step in expanding its utility.

Introduction

Over the past two decades, protein therapeutics have emerged as potent drugs to combat human disease. Their efficacy depends on the intrinsic specificity of proteins for their targets, as well as their mode of action, but many bioactive proteins have limitations that affect their half-life and potency, and thus their overall efficacy. With increased understanding of their function, protein engineering has enabled the construction of modified proteins to address these limitations through conjugations (e.g., pegylation) or by exploiting natural mechanisms for protein retention by half-life extension.[1] Bi- and tri-specific antibodies represent bioengineered molecules that display novel functionality by enabling the binding of two or more antigens. Such molecules have been used, for example, for immune-oncology applications by simultaneously targeting a patient's natural cytotoxic cells and a tumor cell.[2] Antibody-drug conjugates (ADCs) also represent an important class of biotherapeutic that have emerged as a promising treatment for cancer. ADCs combine the targeting specificity of antibodies with potent cytotoxins,[3,4] but unlike bispecific and chimeric proteins, ADCs are obligate conjugates that require the chemical ligation of the drug payload to a protein. The most commonly used conjugation

methods exploit the sulfur group of cysteines or the amine group of lysines. Cysteine-based conjugates, however, have shown instability resulting in a premature release of toxin.[5,6] Likewise, conjugates targeting lysines have been generated using heterobifunctional linkers that contain a succinimide ester and a maleimide. The ester group allows a stable conjugation to the primary amine of lysine residues of the antibody. The maleimide reacts with a sulfhydryl of the payload, forming a thioether that is susceptible to uncoupling by reverse-Michael addition.[7] To address this limitation, site-specific conjugates were developed using engineered cysteines encoded at key sites, which have proven successful in reducing the instability and controlling the drug loads on antibodies.[6,8-11] The reducing conditions needed for cysteine conjugations can also disrupt disulfide bonds necessary for proper protein structure, and therefore are not amenable for use in all proteins.[12] Thus, methods that allow the introduction of unique chemical moieties, enabling bio-orthogonal conjugation chemistries that are not susceptible to uncoupling and do not require conjugation conditions that alter protein structure, have been developed through the incorporation of non-natural amino acids (nnAAs), glycoengineering and enzymatic modifications of peptide tags.[13-23]

The great advantage of nnAAs is the sheer variety of functional chemical moieties, and technologies that are available for site-specific incorporation into proteins.[24,25] While many have been designed to enable conjugation chemistries (e.g., Diels-Alder, click cycloaddition, and by oxime or hydrazone formation),[14-16,26-30] others have been used to examine protein function, protein–protein interactions, protein folding, or to modify enzymatic activity.[31-42] For these technologies, the location of the nnAAs is strategically important to enable both easy and efficient functionalization of the protein, but also to preserve its structural integrity. Expression systems in bacterial, yeast, and mammalian cells, as well as *in vitro* systems, have been developed that offer site-specific incorporation of nnAA with high fidelity.[24] The most popular of these requires the repurposing of a stop codon to encode nnAAs. This is achieved by the heterologous expression of an aminoacyl-tRNA synthetase (aaRS) with specificity for a nnAA, and its cognate tRNA that delivers the nnAA in response to the specified stop codons. This approach enables the site-specific delivery of a nnAA at preselected sites and offers the end user the opportunity to precisely control the site(s) and number of nnAAs.

Several orthogonal aaRS/tRNA pairs have successfully been developed for the incorporation of nnAA in both prokaryotic and eukaryotic expression systems. *Methanocaldococcus jannaschii* TyrRS/tRNAtyr and yeast PheRS/tRNAphe were used for the incorporation of nnAAs in *E.coli*,[43,44] and *E.coli* TrpRS/tRNAtrp was evolved for bacterial and mammalian expression.[45] In addition, prokaryotic LeuRS/tRNAleu and TyrRS/tRNAtyr are commonly used in mammalian and yeast cells.[46-52] The *Methanosarcinna mazei* and *M. barkeri* pylRS/tRNApyl are arguably the most versatile pair that supports nnAA incorporation in bacterial, yeast, *D. melanogaster*, *C. elegans* and mammalian cells.[32,53-58] In each case specific incorporation of a nnAA was observed in response to stop codons. However, expression systems depending on stop codon suppression have historically shown low overall yields. This is due to several factors, including the expression level of the aaRS/tRNA, sequence context of the amber codon, and the function of elongation release factors (RF) that compete with the amber suppressor tRNAs for stop codon recognition[59,60] resulting in premature termination of protein synthesis and production of a truncated protein. This limitation has been addressed in *E.coli* systems in various ways: (1) by genetic mutations of RF-1 to eliminate, or reduce, amber codon recognition;[61] (2) by increasing the aaRS/tRNA levels by optimization of promoter elements, codon usage, or the use of multiple repeats of the aaRS/tRNA in expression plasmids;[62] (3) altering the amber codon sequence context to reduce RF-1 recognition;[63] (4) optimization of the tRNA sequence for improved EF-Tu binding and ribosome recognition;[64-66] (5) through engineering of orthogonal ribosomes specific for the target gene that enable more efficient utilization of amber codons and quadruplet codons;[39] and (6) by expanding the genetic alphabet of cells using unnatural base pairs to assign novel codons to a nnAA.[67] In each case, significant improvements to the yields and efficiency of nnAA-containing proteins were reported.

Mammalian cells are the most common manufacturing platform, offering access to a large variety of protein classes. For the generation of antibodies, mammalian cells are the optimal expression system, as they produce properly folded, functional, and soluble proteins at high yield.[68] Many of the strategies aimed at improving nnAA incorporation listed above are not practical, or simply not possible, in higher eukaryotes. For example, mammalian cells contain a single release factor protein (eRF1) (unlike bacteria which have two) that is essential and recognizes all three stop codons. Thus, stop codon suppression technologies in mammalian cells initially relied on overexpression of the aaRS or tRNA to increase nnAA incorporation efficacy. Studies using transient transfections of mammalian cells determined that high tRNA levels were key to improving nnAA incorporation levels.[54,69,70] Further optimizations have aimed to improve the stability and cross-talk of the tRNA with the mammalian translational machinery,[65,69-71] improve the introduction of the genetic components into cells,[69,72] develop promoters to increase tRNA expression,[54,71] identify permissive sequence context for more efficient amber suppression,[63] as well as overexpress mutant eRF1 with reduced affinity for amber codons.[70] These optimizations have led to significant improvements in the yields of mammalian cells, and more importantly identified key components that affect the efficiency of nnAA incorporation.

Transient transfections of mammalian cells can be used to generate antibodies with nnAAs, but while yields are relatively low, sufficient material can be generated for characterization. In order to reproducibly achieve high productive yields with consistent product quality compatible with manufacturing requirements, stable cell lines are required. One major limitation of mammalian cells in the context of nnAA incorporation is that, unlike bacterial expression systems in which protein production can be completed within a few hours, mammalian expressions require up to 14 days to maximize the production yields. Prolonged amber suppression is thought to be deleterious to cells, resulting in early loss of viability and thus reduced expression times. Nevertheless, high producing platforms capable of g/L yields of nnAA-containing antibodies have been reported.[15,18,] In these cells the orthogonal aaRS and multiple copies of its cognate tRNA were introduced and cells functionally selected. While we have a good understanding of the mechanism behind nnAA incorporation, we do not yet understand the minimal expression requirements of aaRS and its tRNA needed to support the prolonged and high titer expression of stable expressers.

Here we describe the steps used for the generation of a host platform in Chinese hamster ovary (CHO) cells to produce biotherapeutics containing nnAAs, and for the first time, identify the critical components needed for high efficiency of nnAA incorporation. We also show that the process is robust, resulting in the generation of two platform host lines that are each capable of high titer expression of nnAA-containing IgG. Furthermore, we developed a scale-up process that is compatible with established upstream platform perfusion processes, suitable for manufacturing and commercialization.

Results

Generation of stable platform hosts for the incorporation of non-natural amino acids

The incorporation of a nnAA requires engineered cells expressing an orthogonal aaRS/tRNA pair with specificity for the nnAA. In an effort to generate a highly efficient system, we generated stable platform hosts expressing the pyrrolysine tRNA synthetase (pylRS) and its cognate tRNA (tRNApyl) derived from archaebacterial *Methanosarcina mazei*, an enzyme previously shown to mediate nnAA incorporation in mammalian cells.[18,54] Stable cell lines armed with this system are a desirable tool for manufacturing because it represents the starting point for the construction of expression cell lines. First, we constructed a vector bearing expression cassettes for PylRS under the control of a CMV promoter, as well as 18 tandem repeats of tRNA under the U6 snRNA promoter. The vector also contained a puromycin selection marker for stable cell line selection. Following transfection into AstraZeneca-proprietary suspension CHO cells, the transfectants were plated in 96-well plates and subjected to selection in puromycin-containing media.[73,74] Surviving colonies were expanded and screened for amber suppression activity using a high throughput functional assay. This required the transfection of an mRNA reporter probe encoding a red fluorescent protein (RFP)-green fluorescent protein (GFP) fusion containing an amber codon between the two genes (RFPamb-GFP) (Figure 1a).[75,76] Transfected cells were exposed to the nnAA (S)-2-amino-6-((2-azidoethoxy) carbonylamino) hexanoic acid (Figure 2a, AzK) to enable amber suppression. With this probe, all transfected cells express RFP, but only cells capable of amber suppression (and nnAA incorporation) also express the GFP reporter (Figure 1b).

Fluorescent protein expression was quantified by flow cytometry in a total of 384 colonies. Two criteria were applied to assess the amber suppression activity. The colonies were ranked based on: 1) the ratio of the geometric means of GFP (amber suppression) to RFP (total expression) (Figure 2b), and 2) the percentage of dual positive cells (Figure 2c). Among the top 50 candidate hosts, 35 platform hosts showed reasonable growth properties and amber suppression activity. These were further screened for stable IgG expression in pool format using an IgG expression plasmid containing an amber codon in the variable domain of the heavy chain (HC) at position 44 (IgGamb), as well as encoding the light chain of the IgG, and the glutamine synthetase (GS) selection marker.[77] With this construct, only cells capable of amber suppression produce a secreted antibody that can be quantified from the growth medium. While most of the hosts were amber suppression positive, based on the mRNA reporter assay, very few showed high titer IgG expression (Figure 2d). Indeed, only pools from three hosts (#27, 38 and 43) demonstrated IgG titers above 100 mg/L, and only one pool from host 43 was capable of producing titers exceeding 1 g/L. Despite the high level of amber suppression activity in this host in medium containing nnAA, no disadvantage in growth was observed in its absence, relative to the parental cell line.[75] These data show that, while the fluorescent reporters are useful tools to identify amber suppressors and reduce the screen size, screening by IgG expression was critical for finding high-performance amber suppression platform hosts.

Genetic characterization of nnAA platform hosts

To learn what factors govern the efficiency of amber suppression, we quantified the gene copy number and mRNA
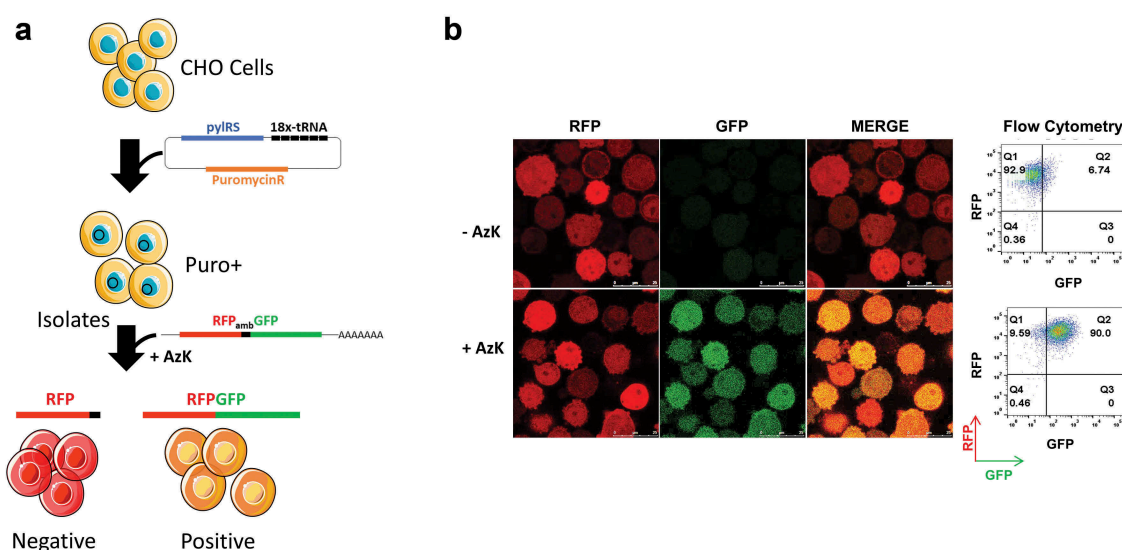
Figure 1. mRNA reporter assay for screening amber suppression positive stable isolate hosts. (a) Schematic representation of the process used to generate and identify amber suppression competent cells. CHO cells were first transfected with a plasmid encoding PylRS and tRNApyl and subjected to a selection step by growth in puromycin-containing medium. Surviving isolates were transfected with mRNA encoding RFPambGFP and cells were exposed to AzK. Cells capable of efficient amber codon suppression (positive) express an RFP-GFP fusion and are positive for both fluorophores. Cells lacking amber suppression activity (negative) express only RFP. (b) A stable isolate identified as positive for amber suppression activity was transfected with the RFPambGFP mRNA and incubated in the presence or absence of AzK. Cells were imaged by confocal microscopy and flow cytometry. Amber suppression and incorporation of AzK was observed in presence of PylRS and tRNApyl. No GFP expression was observed in absence of AzK.
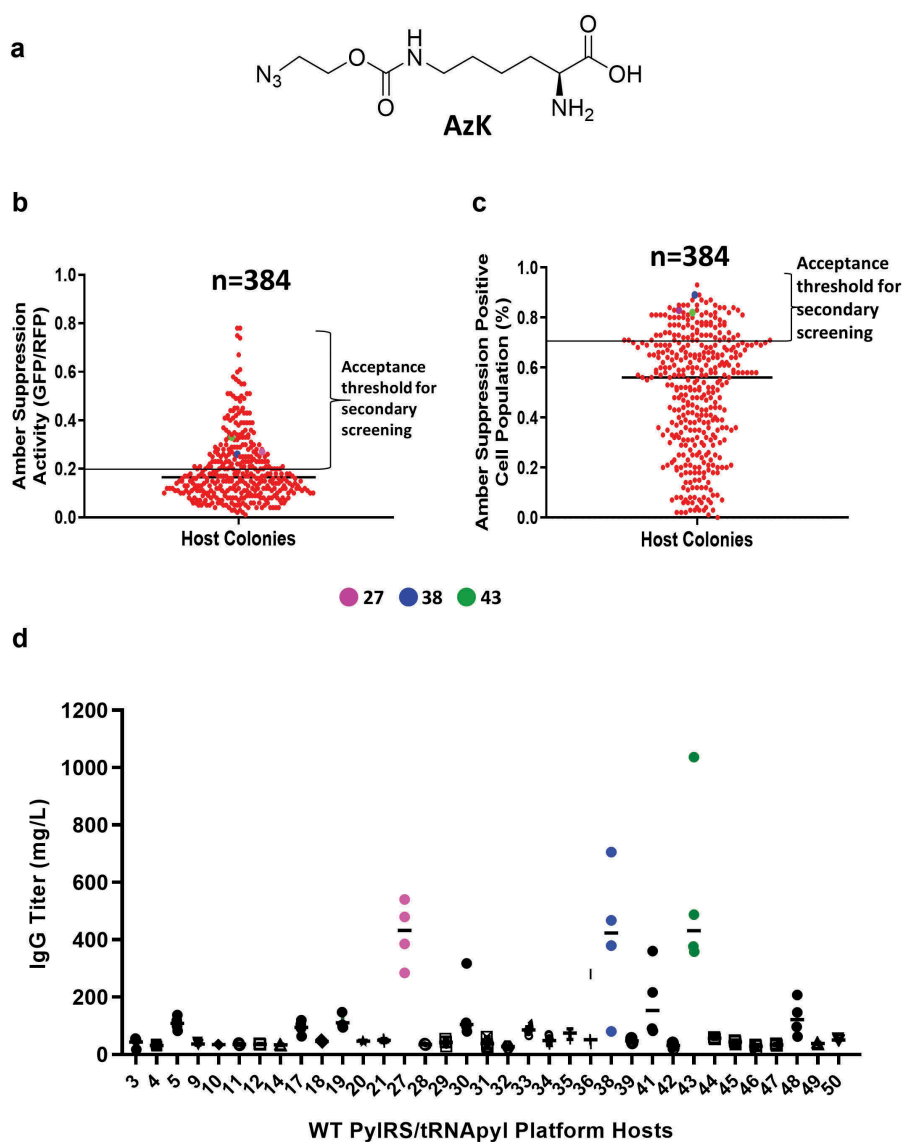
Figure 2. **Screening criteria for selection of amber suppression efficient hosts.** (a) Structure of AzK. (b) Ranking of platform hosts based on amber suppression activity determined by the ratio of mean fluorescence intensity of GFP to RFP (GFP/RFP) or (c) based on the percentage of the population showing dual fluorescence protein expression. The relative ranking of the three top hosts based on IgG expression are indicated with pink (27), blue (38) and green markers (43). (d) Isolates identified as positive for amber suppression (n = 50) were assessed for amber codon dependent IgG expression. Candidate hosts were transfected with IgGamb and four pools from each candidate assessed for IgGamb titer in the presence of AzK. Titer values for each pool were plotted with median expression shown. Host candidates 27, 38 and 43 showed the highest IgGamb expression levels and were selected for further evaluation.

expression of tRNApyl and PylRS by quantitative polymerase chain reaction (QPCR) in both high and low IgG-expressing platform hosts (Table 1).[76] Since the pylRS and tRNApyl genes are linked, it was not surprising to find a correlation between PylRS and tRNApyl gene copy numbers (R-square value of 0.9). Indeed, the pylRS:tRNApyl ratios of approximately 1:18,

Table 1. Genetic characterization of amber suppression platform hosts.

| Host ID	Average doubling time (h)	PylRS Copy Number	tRNApyl Copy Number	PylRS expression ratio to 18s	tRNApyl expression ratio to 18s	% Mature tRNA	% Unprocessed tRNA	Top pool titer (mg/L)
Parental CHO	33.3	N/A	N/A	N/A	N/A	N/A	N/A	N/A
53	25.3	2.2	42.4	0.0045	1.54	85.6	14.4	137
174	39.6	0.8	14.6	0.0036	1.12	96.1	3.9	119
19	27.6	1.2	18.0	0.0034	0.52	95.4	4.6	147
27**	30.0	4.6	196	0.0186	6.1	97.2	2.8	540
30	30.1	1.2	22.3	0.0027	1.09	95.7	4.3	317
33	24.5	0.3	7.2	0.0023	0.63	95.6	4.4	90
38**	28.0	7.2	311	0.0335	15.5	96.3	2.7	705
41	33.4	0.5	7.5	0.0019	0.34	96.2	3.8	360
43**	28.4	11.5	357	0.0341	9.2	93.5	6.5	1036
48	46.9	1.3	26	0.0056	0.42	86.8	13.2	207

** Top three hosts based on genetic characteristics and IgG titer

encoded in the input plasmid, were observed in most of the hosts except for hosts 27, 38 and 43, where the tRNApyl gene copy numbers were elevated relative to the PylRS. Interestingly, mRNA analyses revealed that these hosts also showed elevated tRNApyl and PylRS expression and the highest IgGamb titers, suggesting that higher system expression improves amber suppression potential. In addition, a high correlation (R-square value of 0.9) between gene copy numbers and IgG titer was observed (Figure 3a,b). In an effort to improve the homogeneity of the host populations and to isolate clonal platform hosts with the highest potential for amber suppression, a round of cloning was conducted using ClonePix FL[77] and derived clones were characterized for amber suppression efficacy as described above. Thus, clones isolated from host 43 were expanded and both tRNApyl and pylRS copy numbers and IgGamb titers were determined (Figure 3c,d). The isolated clones contained about 10 PylRS genes, between 200 and 300 tRNApyl genes, and supported IgG expression levels of >1.2g/L. This is in line with previous estimates for highly efficient amber-suppressing cells.[69] The top clonal host, with an IgGamb pool titer of 2.0 g/L, contained the highest copy number for tRNApyl (>600 copies) and PylRS (>25 copies). The correlation between the tRNApyl and PylRS copy number and IgG titer among the clonal hosts was reduced (R-squared of 0.68), possibly due to the less diverse nature of the parental host 43 contributing to the cluster of clonal hosts with similar tRNApyl and PylRS copy numbers, as well as IgG productivity. These data clearly show that elevated PylRS/tRNApyl gene copy numbers and expression levels support higher amber suppression activity and point to PylRS and tRNApyl copy number analyses as a key metric for characterizing platform hosts.

Characterization of IgG expressing cell lines generated in nnAA host platforms

Having identified platform hosts capable of amber suppression and high titer expression of IgGamb, we set out to quantify the efficiency of nnAA incorporation in stable IgGamb cell lines generated from these hosts. To do this, we stably expressed IgG in two different hosts containing high (host 43) and low (host 27) copy numbers for tRNApyl and PylRS. The IgG expression construct contained an amber codon at heavy chain position K274 that generates a truncated IgG in the absence of amber suppression, but upon readthrough of the amber codon, a full-length IgG is produced. Because the antibody used contains a Fab-HC belonging to the VH3 family, capable of protein A binding, the full-length IgG (detected using Fc-specific antibodies) and total IgG (detected using protein A sensors) could be quantified by biolayer interferometry with separate assays. Thus, the ratio of full-length/total IgG reflects the efficiency of nnAA incorporation by the system. Cell performance of the primary isolates were assessed by monitoring viable cell density (VCD) (Figure 4a), viability (Figure 4b), and IgG titers for both full-length and truncate forms over a 14-day fed-batch expression using AstraZeneca-proprietary media and nutrition-enriched feed (Figure 4c). Amber suppression was induced by the addition of 2 mM AzK to the medium on day 4 of the fed-batch culture.

We observed that IgG-expressing cell lines derived from host 27 and 43 maintained high VCDs and cell viability during the fed-batch process (Figure 4a,b). All expresser cell lines tested produced equivalent levels of total IgG (1.3–1.6 g/L). The cell
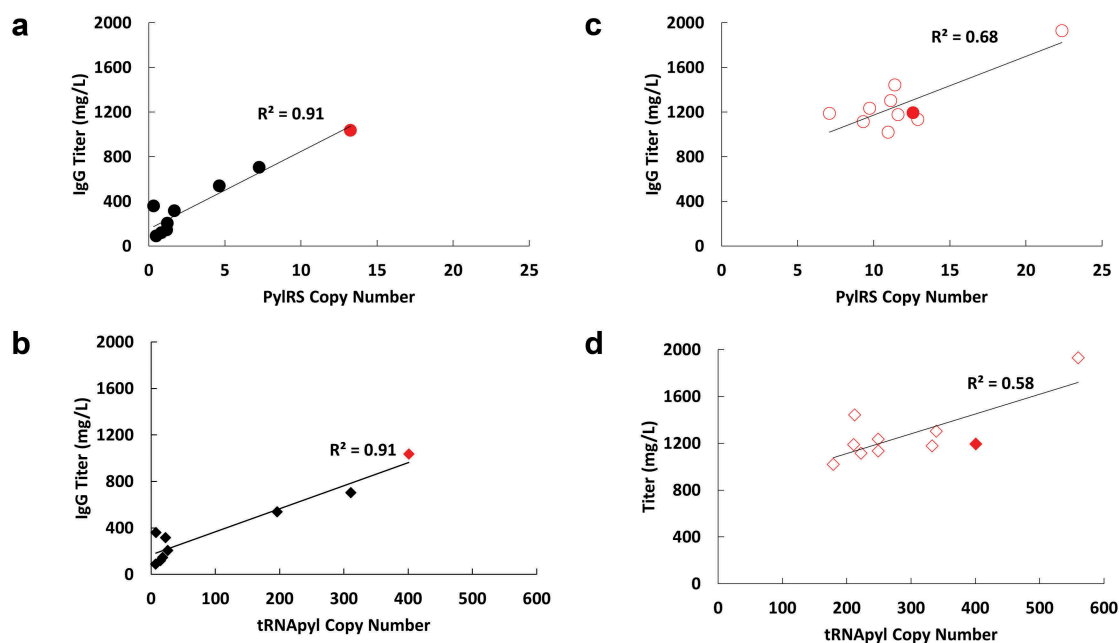
Figure 3. Correlation between PylRS and tRNApyl copy numbers and IgG Titer. (a) Correlation between PylRS gene copy number and IgG titer of the isolated host platforms. The red marker indicates host 43. (b) Correlation between tRNApyl copy number and IgG titer of the isolated host platforms. The red marker indicates host 43. (c) Correlation between PylRS gene copy number and IgG titer of 10 clonal hosts derived from host 43 (solid red). (d) Correlation between tRNApyl copy number and IgG titer of the 10 clonal hosts derived from host 43 (solid red).
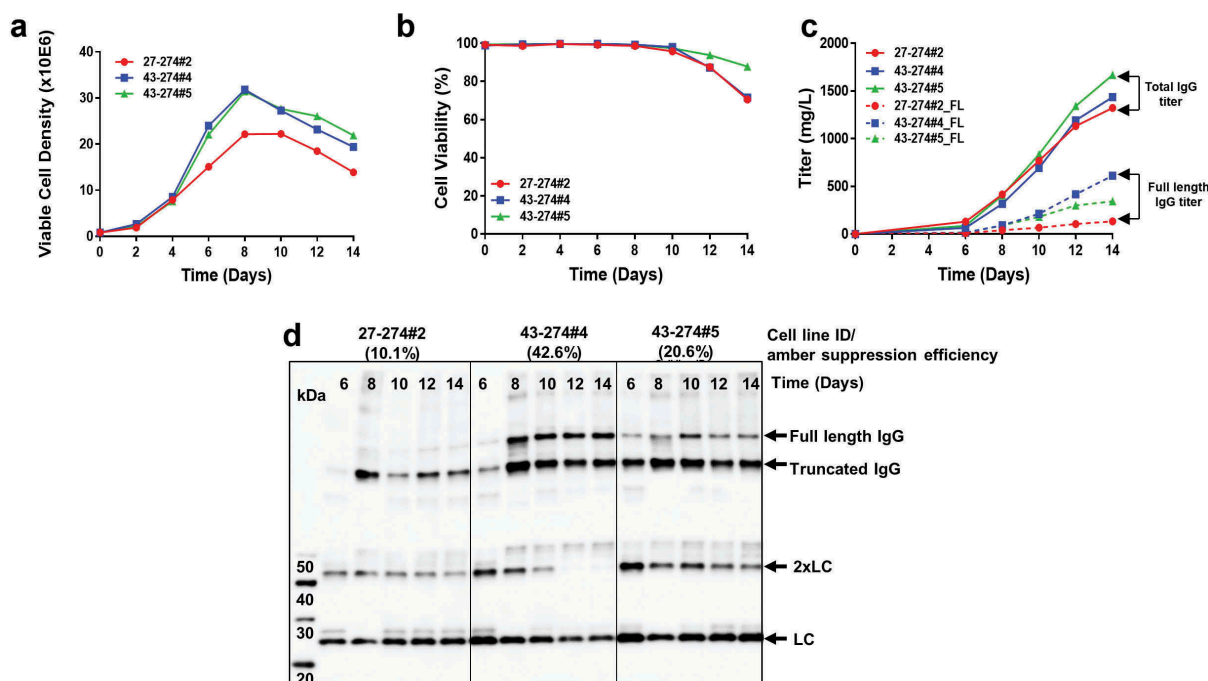
Figure 4. Cell growth and productivity profiles of different IgG-expressing stable lines containing different levels of amber suppression activity. Expression cell lines derived from C13–27, and −43 were generated and subjected to a 14-day fed-batch expression. For each cell line we determined: (a) viable cell densities, (b) cell viability, and (c) full length and truncated IgG titer. (d) Crude supernatants from each fed-batch culture were resolved under non-reducing condition by SDS-PAGE and analyzed by Western blotting using an antibody that recognizes the truncated and full-length IgG. The positions of full-length and truncated IgG heavy chain, light chain (LC) and light chain dimers (2xLC) are indicated. The efficiency of amber suppression in each culture was calculated after quantifying full-length and truncated IgG levels by surface layer interferometry.

Table 2. pylRS and tRNA expression analysis and amber suppression efficacy of top three platform hosts.

Cell Line ID	tRNApyl Copy Number	PylRS Copy Number	Total IgG Expression (mg/L)	Full Length IgG Expression (mg/L)	Amber suppression efficiency
27–274#2	89.6	3.1	1322	134	10.1%
43–274#4	280.2	10.6	1436	613	42.6%
43–274#5	161.2	6.0	1668	344	20.6%

**Expression ratios are expressed relative to β2M expression

line derived from host 27 (27–274#2), containing only 89 copies of tRNApyl and 3 copies of PylRS (Table 2), produced 134 mg/L of full-length IgG, representing an amber suppression efficiency of 10% (Figure 4c). Western blot analyses of crude supernatants show that the majority of the product is truncated IgG, whereas the full-length IgG is almost undetectable (Figure 4d). Interestingly, cell line 43–274#4 derived from host 43, containing 280 copies of tRNApyl and 10 copies of PylRS (Table 2), showed 42% amber suppression efficiency and produced much higher levels (613 mg/L) of full-length IgG (Figure 4c) that is clearly detected by Western blotting (Figure 4d). The third cell line 43–274#5, containing 161 copies of tRNApyl and 6 copies of PylRS, (Table 2) showed a 20% amber suppression activity and produced 344 mg/L full-length IgG (Figure 4c). The genetic characteristics of the cell lines, full-length and truncated IgG expression levels, and their corresponding amber suppression activity are summarized in Table 2. Interestingly, the differences in amber codon suppression efficiency were not related to lack of tRNApyl maturation, as all cell lines demonstrated equivalent levels (~85%) of mature (processed) tRNApyl (Table 3). However, it is clear from these data that the copy number and expression levels of tRNApyl and PylRS determine amber suppression efficiency.

Table 3. tRNA and pylRS expression analysis of IgG (K274 amber) stable expressers.

Cell Line ID	Processed tRNApyl Expression Ratio	Unprocessed tRNApyl Expression Ratio	Mature to Unprocessed tRNA Ratio (%)	PylRS Expression Ratio
27–274#2	0.0296	0.0035	88%:12%	0.00004
43–274#4	0.0956	0.0150	84%:16%	0.00006
43–274#5	0.0296	0.0044	85%:15%	0.00003

**Expression ratios are reported relative to 18S expression

Host platform generation with mutated PylRS and tRNApyl for expansion of repertoire of nnAAs incorporation in protein sequences

To expand the repertoire of nnAAs that can be introduced into proteins, we applied the same screening strategy to generate hosts capable of introducing nnAAs containing cyclopentadiene moieties such as CpHK and SCpHK (Figure 5a).[78] These lysine derivatives enable Diels-Alder cycloaddition, a rapid, metal free, and efficient reaction useful for the conjugation to dienophile bearing payloads (e.g., maleimide). The incorporation of CpHK and SCpHK, however, requires a PylRS containing a mutation (Y306A) that
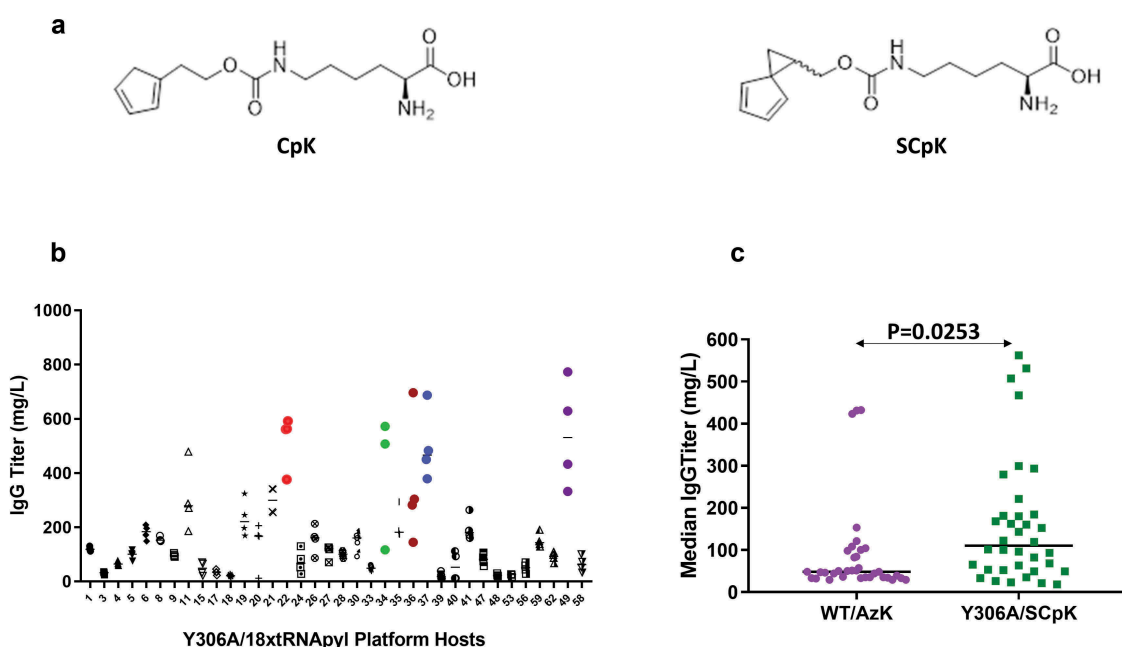
Figure 5. **Screening strategy yields efficient PylRSY306A mutant host**. (a) Distribution of IgG titer in stable pools generated in Y306A and tRNApyl expressing platform hosts. Best performing hosts are shown with colored markers. (b) Median IgG titers of stable pools generated from WT and Y306A host platforms were plotted. Y306A host cells show improved median expression levels of full-length IgGamb.

expands the amino acid binding pocket, enabling the capture of CpHK and SCpHK. Thus, a plasmid encoding pylRSY306A (Y306A) and 18 tRNApyl repeats was constructed and stably transfected into AstraZeneca-proprietary suspension CHO cells.[73,74] Transfected cells were selected and characterized as previously described. Figure 5b shows the titer distribution of stably expressed IgGamb in stable pool format. Four platform hosts produced more than 500 mg/L IgG (IgGamb containing an amber codon at position HC44 was used) from stable pools (Figure 5c). The comparison of the platform host generation process expressing the wildtype (WT) and Y306A is summarized in Table 4. The screening profiles for the generation of highly active amber suppression-enabled host platforms show the reproducibility of the screening strategy. It also suggests that finding hosts with high amber suppression activity is a rare event and requires high throughput functional screening. The genotypic and phenotypic characteristics of the four top Y306A hosts are summarized in Table 5. Based on the IgG productivity, PylRS and tRNApyl copy numbers, and

population doubling time, host Y306A36 was chosen for further development as a manufacturing host. Interestingly, the Y306A hosts were shown to incorporate both CpHK and SCpHK as well as AzK, albeit with lower efficiency, making these hosts useful for the characterization of different conjugation chemistries.

Stability of nnAA platform hosts for amber suppression activity and IgG expression

The stability of an expression host is an important consideration for the selection of a manufacturing platform to ensure consistent production levels and product quality. To evaluate this the top platform hosts for each of our campaigns, hosts 27, 38 and 43, the top three clonal hosts 43#3, 43#8 and 43#37, and Y306A36 were routinely passaged and cells were cryo-preserved after 10 (E, early) and 60 (L, late) population doublings (PDLs). Each of the cryopreserved platforms were revived and stably transfected with an IgGamb expression construct encoding IgG containing an amber codon at

Table 4. Comparison of host identification metrics from two independent cell line engineering campaigns.

Host platform	Total colonies screened	Positives post functional screen	Screened by IgG expression	Number of potential good hosts	Positive hits (%)
WT	384	50	35	3	0.78
Y306A	216	64	38	5	2.3

Table 5. pylRS and tRNA expression analysis for top pylRSY306A hosts.

Host ID	Average doubling time (h)	PylRS Copy Number	tRNApyl Copy Number	PylRS expression ratio to 18s	tRNApyl expression ratio to 18s	% Mature tRNA	% Unprocessed tRNA	Top pool titer (mg/L)
Y306A22	39.3	5.3	210.0	0.0018	0.94	94.4	5.6	592
Y306A36	38.1	10.3	343.0	0.0014	0.97	86.2	13.8	696
Y306A37	42.1	30.9	1103.2	0.0071	2.73	92.7	7.3	687
Y306A49	45.9	12.7	469.6	0.0043	1.92	92.8	7.2	773

position 44 of the HC. Twelve IgGamb expressing stable pools were generated and evaluated for productivity (Table 6). We observed a decrease in the productivity of cells with increased PDL. The platform Y306A36 was an exception, retaining its productivity even after 60 PDLs. To better understand the mechanism behind this drop in productivity, we assayed each platform for tRNApyl and PylRS copy number. WT PylRS hosts 27 and 38 lost PylRS and tRNApyl copies over 60 generations and were not evaluated further for IgG expression (Table 6). The host 43 showed a 27% drop in tRNApyl and PylRS genes copy numbers in late passage cells, which contributed to a nearly 40% drop in average titer in stable pools. Whereas 43#8 showed stability in the PylRS and tRNApyl copy numbers, the mean IgG titer dropped almost 50% in late, compared to early passage cells, even though the specific productivity (QP) remained consistent (Supplemental Figure 1d). The drop in overall titer was associated with reduced growth rate and early cell death of the late passage cells in a 14-day fed-batch expression (Supplemental Figure 1a and b). The Y306A36 host retained its PylRS and tRNApyl copy numbers and IgG productivity in stable pools. The drop in tRNApyl and PylRS mRNA expression and increased levels of unprocessed tRNApyl in late passage cells of Y306A36 host did not affect the median titers of the stable IgG pools.

Process development strategies for IgG production using nnAA hosts in perfusion bioreactors

The use of orthogonal aaRS/tRNA for the incorporation of nnAAs has proven to be a very precise method for delivering a nnAA at preselected sites. However, the major limitation of nnAA technologies has been the low productivity in cell-based systems. Previous reports demonstrating >1g/L yields show that the limitations of this system can be overcome in stable cells and with careful cell line selection.[15,18] To further improve the robustness of this system, and further increase the expected overall titers, we developed a process for the expression of nnAA-containing proteins using perfusion bioreactors. Perfusion systems allow for the addition of fresh media and nutrients and the simultaneous removal of cell waste to maintain optimal growth and expression conditions. Thus, stable cel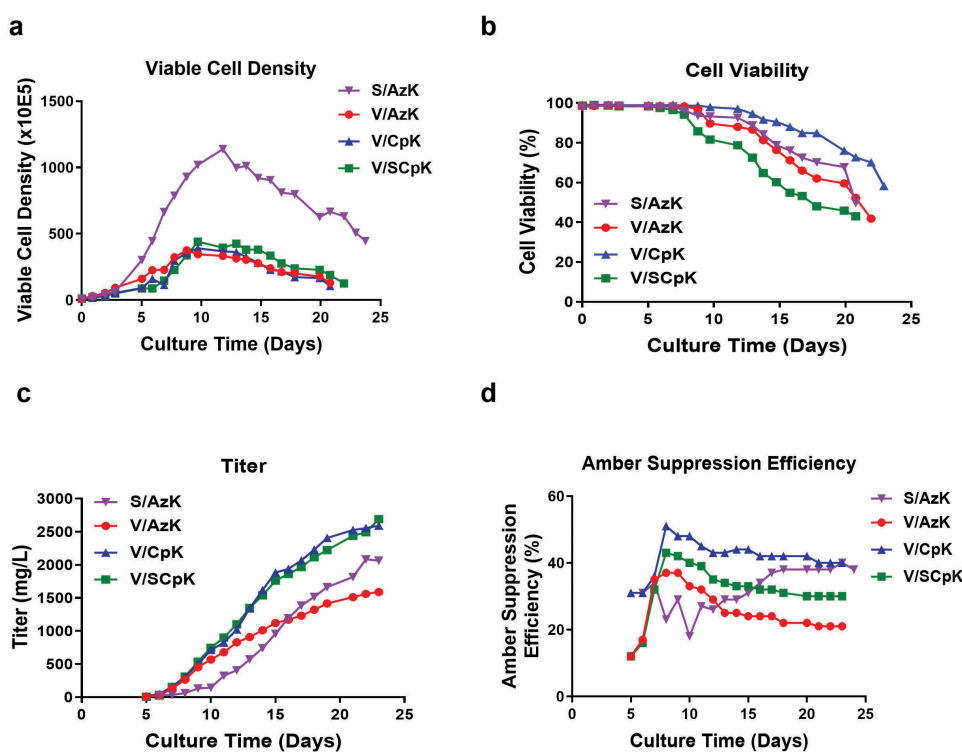ls expressing an antibody directed against human epidermal growth factor receptor 2 (HER2)/neu, containing an amber codon encoded in the antibody constant heavy domain 2 (CH2), were generated in host 43 and Y306A36 hosts and IgG-expressing stable primary isolates were subjected to perfusion fermentations. The site of incorporation can affect expression levels of the system; in this assessment, we selected a CH2 domain site that represents a challenging position for incorporation efficiency and is functionally significant for ADC assembly. The expression line derived from host 43 was exposed to AzK (S/AzK), and the expression cell line derived from Y306A36 was exposed to either AzK (V/AzK), CpHK (V/CpHK) or SCpHK (V/SCpHK) starting on day 5 of the fermentation.

In each culture, the antibody productivity, amber suppression efficiency, cell viability, and viable cell density (VCD) were monitored over a 24-day period (Figure 6a-d). We observed that S/AZK achieved very high cell densities (1×10^8 cells/mL), whereas the V/AzK, V/CpHK and V/SCpHK maintained a VCD of 5×10^7 cells/ml (Figure 6a). The high VCD of S/AzK cell line is most likely related to the characteristics of the platform host and independent of the nnAA incorporation system. Nevertheless, perfusion fermentation allows the generation of a higher biomass than is typically achieved by conventional methods ($1-10 \times 10^6$ cells/mL). Despite the high cell densities, the viability of all the cultures was maintained above 80% for 10 days with a gradual decline over the remaining period. It should be noted that V/SCpHK cells showed an earlier decline than other cultures (Figure 6b). This more rapid decline however, was not related to the efficacy of amber suppression (calculated as $\frac{\text{Full length IgG}}{\text{Total IgG (Trunctaed + Full length)}}$), as V/CpHK showed a higher efficiency of nnAA incorporation than other cell lines. Although, the amber suppression efficiency was higher in V/CpHK (40%) compared to V/SCpHK (23%) (Figure 6d), the full-length IgG normalized productivity of both cell lines was 3.0 g/L. Due to the lower efficiency of AzK incorporation by the Y306A36 host, V/AzK showed a lower efficiency (20%) than other cells and resulted in a normalized titer of 1.5 g/L (Figure 6c). AzK incorporation in S/AzK was also around 40% efficient (Figure 6d) and produced about 2.5 g/L of full-length IgG (Figure 6c).

Table 6. Stability of pylRS and tRNApyl expression in early and late passage populations.

Sample	tRNApyl Copy number	PylRS Copy number	tRNApyl expression ratio	PylRS expression ratio	Matured tRNApyl	Unprocessed tRNApyl	Average pool titer (mg/L)
27E	196	4.6	1.50	0.0046	96.9%	3.1%	N/A
27L	69	2.2	0.02	0.0001	72.1%	27.9%	N/A
38E	311	7.2	1.36	0.0048	95.6%	4.4%	N/A
38L	71	2.3	0.30	0.00004	83.7%	16.3%	N/A
43E	259	8.8	1.40	0.0014	95.7%	4.3%	878.8 ± 214.0
43L	194	6.5	1.43	0.0019	96.1%	3.9%	528.2 ± 153.4
43#3E	239	9.8	1.46	0.0013	88.3%	11.7%	742.2 ± 236.5
43#3L	166	6.2	0.65	0.0006	89.5%	10.5%	379.5 ± 60.3
43#8E	224	9.1	1.22	0.0010	92.2%	7.8%	1144.6 ± 271.9
43#8L	285	12.1	1.22	0.0005	95.9%	4.1%	542.4 ± 82.2
43#37E	445	16.4	0.46	0.0007	91.0%	9.0%	799.5 ± 203.8
43#37L	126	4.7	0.25	0.0004	93.3%	6.7%	138.9 ± 36.42
Y306A 36E	377	12.8	1.20	0.0016	90.1%	9.9%	315.0 ± 84.0
Y306A 36L	354	14.8	0.64	0.0008	85.9%	14.1%	462.1 ± 127.5

Figure 6. Monitoring of cell performance, amber suppression efficiency and titer distribution during perfusion bioreactor process development. Viable cell density (a), cell viability (b), full-length IgG titer (c) and amber suppression efficiency (d) were measured in anti-HER2 IgG-expressing cell lines S/AzK, V/AzK, V/CpHK and V/SCpHK in perfusion mode. S/AzK is expressed in WT PylRS/tRNApyl platform host while V/AzK, V/CpHK and V/SCpHK represents a cell line derived from the Y306A/tRNApyl platform host and induced with AzK, CpHK and SCpHK nnAAs.

IgG produced by the perfusion process shows efficient conjugate formation and potency *in vitro*

To demonstrate that the products of the perfusion expressions efficiently generated antibodies with site-specific nnAA incorporation, the IgG products were subjected to a conjugation reaction with the toxin tubulysin. To do this, each perfusion culture was collected, and the antibodies purified by affinity chromatography. The purified antibodies were then combined with tubulysin payloads armed with linker groups that allow specific conjugation chemistries for the integrated nnAAs, maleimide (for conjugation to CpHK and SCpHK) or dibenzylcyclooctyne (DBCO) (for conjugation to AzK). Due to the increased mass of antibody-drug adducts, HC conjugates show a retardation in gel mobility that is readily observed by SDS-PAGE and Coomassie staining. We observed efficient conjugate formation in all cases, suggesting efficient nnAA incorporation (Figure 7a). Furthermore, the deconvoluted masses of reduced antibodies, and their corresponding ADCs, measured by mass spectrometry, show mass differences that are consistent with the addition of the corresponding payloads (difference of 1074.6 Da for monoclonal antibodies (mAbs) with AzK and 1091.6 Da for mAbs with CpHK or SCpHK). The data also show that the reactions are complete, and that each HC was modified by a single warhead (Figure 7b). The site-specific nnAA incorporations and conjugations were confirmed by peptide mapping. Nonspecific conjugation was not observed (Supplement Figure 2).

The glycoforms for naked antibodies and their corresponding ADCs from peptide mapping data are summarized in Table 7. Interestingly, the major glycoforms are fucosylated biantennary structures (G0f, G1f, G2f) without sialic acid for the host 43-derived expresser and with sialic acid (G1f+NAc, G2f+NAc, G2f+2NAc) for the Y306A-derived cell line. However, there is no difference in glycan profiles before and after conjugation for all samples. Further characterization of IgG products derived from other Y306A platform hosts suggests that the excess sialylation was an independent characteristic of host Y306A36 platform and unassociated with the introduction of the PylRS gene.

The constructed ADCs were tested to assess their potency and specificity *in vitro*. For these assays, HER2-positive SK-BR-3 and HER2-negative MDA-MB-468 cell lines were cultured *in vitro* with the indicated ADCs and controls, and their viability assessed after 3 days (Figure 7c). The data show that all the anti-HER2 ADCs are cytotoxic to high Her2-expressing cells, SK-BR-3 (IC50 = 4–7ng/ml), but greatly reduced toxicity to HER2-negative cells, MDA-MB-468 (IC50 >3600ng/ml) (Table 8).

Table 8. In vitro potency (IC50 ng/mL) of Tubulysin conjugates on Her2-positive Sk-Br-3 cells.

IgG sample	Payload (Tubulysin)	IC50 (ng/ml)
HER2 S/AzK	+	4.08
HER2 V/AzK	+	7.25
HER2 V/CpK	+	5.71
HER2 V/SCpK	–	429
HER2 V/SCpK	+	4.82
R347/AzK	+	>3600
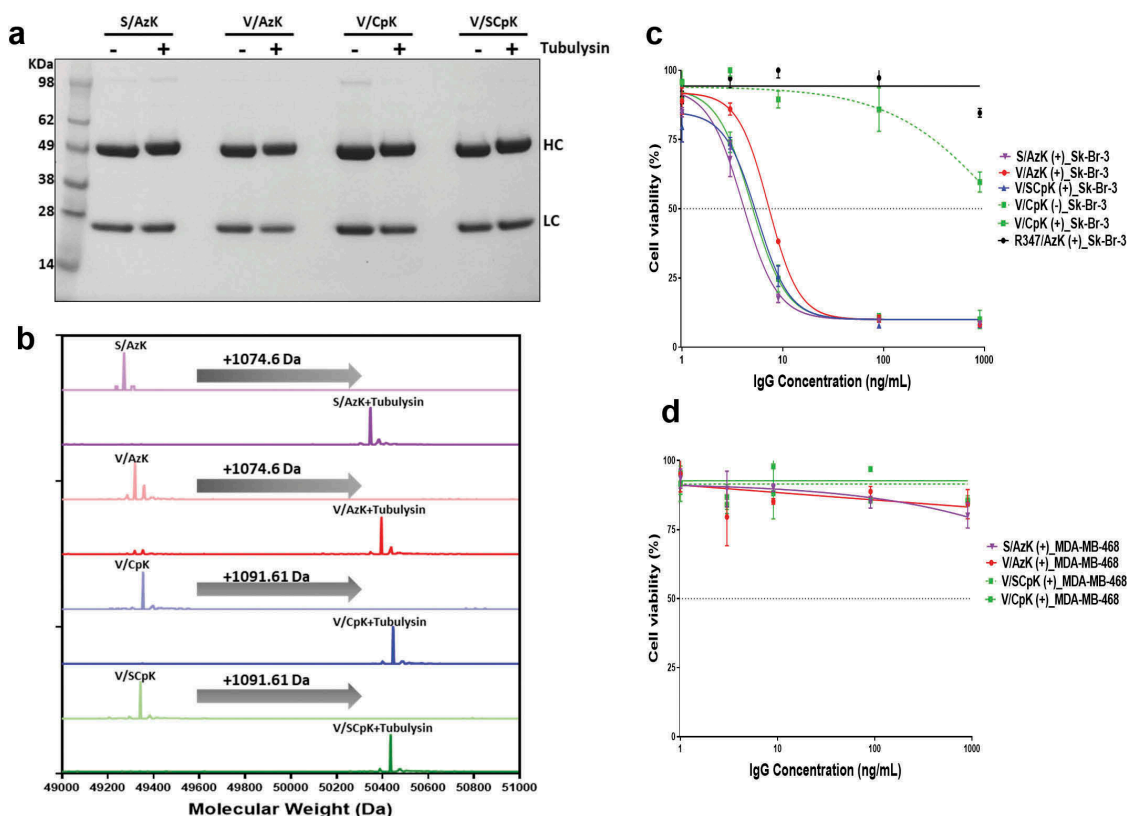
Figure 7. Functional assessment of nnAA bearing antibodies. Antibodies purified from each of the perfusion cultures were purified and characterized for conjugation efficacy and ADC function. (A) Affinity-purified antibodies were conjugated to tubulysin warheads containing alkyne- (DBCO; for AzK IgGs) or maleimide- (for SCpHK and CpHK) bearing linkers. Unconjugated (-) and conjugated samples were resolved by SDS-PAGE and stained with Coomassie. A retardation in gel mobility is observed in the HC, but not the LC, of conjugated samples, suggesting near-complete conjugate formation. (b) Reduced antibodies and ADCs were analyzed by mass spectrometry. ADCs show an intact HC mass increase corresponding to the mass of the DBCO-tubulysin (1074.6 Da) or maleimide-tubulysin (1091.61 Da) adducts indicating the addition of a single payload to the HC. No unreacted material was observed in ADC samples. **C. and D**. The constructed ADCs were functionally tested in an in vitro cytotoxicity assay. Antibodies and ADCs were incubated with HER2 positive (Sk-Br-3) (c) and negative (MDA-MB-468) (d) cell lines and their viabilities were assessed. V/CpHK (-) in **C** represents HER2 mAb without a toxic payload. All ADCs show potent and specific on target killing.

Table 7. Glycosylation profiles of antibodies generated by nnAA host cells.

Glycoforms	S/AzK	S/AzK+ Tubulysin	V/AzK	V/AzK+ Tubulysin	V/CpK	V/CpK+ Tubulysin	V/SCpK	V/CpK+ Tubulysin
G0-GN	2.9	2.8	1.5	1.1	1.4	1.5	2.0	2.2
G0f-GN	3.6	3.6	3.1	4.9	2.6	2.7	3.4	3.7
G1-GN	1.2	1.2	0.4	0.5	0.3	0.3	0.4	0.4
G1f-GN	1.9	2.0	2.6	6.1	1.3	1.5	1.7	1.8
G1f-GN+NAc	0.5	0.4	2.1	2.7	1.0	0.8	1.3	1.0
G0	8.1	8.1	0.4	0.4	0.3	0.2	0.4	0.3
G0f	40.8	40.8	6.2	5.1	5.7	5.1	5.1	6.0
G1	2.9	2.9	0.6	0.6	0.5	0.5	0.6	0.7
G1f	22.8	22.8	16.6	16.1	17.1	18.9	18.3	20.0
G2f	3.8	3.8	13.6	15.4	14.5	16.3	14.0	14.8
G1f+NAc	0.1	0.1	7.1	5.8	9.3	9.4	8.8	8.8
G2f+NAc	0.3	0.3	17.2	16.6	19.6	19.9	16.8	16.7
G2f+2NAc	0.1	0.2	16.3	13.9	16.2	16.6	13.7	13.7
M3	1.5	1.4	0.7	1.3	0.1	0.1	0.2	0.2
M5	10.1	9.9	10.2	11.6	8.0	8.1	10.9	11.3
M6	0.9	1.0	0.7	0.8	0.9	1.0	1.1	1.2
M7	0.4	0.4	0.2	0.2	0.4	0.4	0.4	0.4
M8	0.2	0.1	0.2	0.2	0.3	0.3	0.4	0.4
aglycosylation	3.3	4.0	1.0	1.1	1.2	1.2	1.0	1.1

**S/AzK was generated in host 43 expressing WT PylRS whereas N/AzK/CpK/CpK were generated in Y306A36 host expressing mutant PylRS

Moreover, a non-HER2 targeting control antibody (R347) expressed to contain AzK and conjugated with tubulysin demonstrated low cytotoxicity to SK-BR-3 cells (IC50 > 3600). These data collectively demonstrate the high potency and specificity of cytotoxicity of the conjugated mAbs derived from both WT and Y306A platform hosts.

Intracellular localization and detection of PylRS in secreted mAb and purified IgG samples

The overexpression of PylRS in manufacturing host cell lines raises an immunogenicity risk if this archaebacterial-derived protein contributes to the host cell protein load in a mAb

a

FLAG-PylRS   Atp1a1   DAPI   Overlay

b
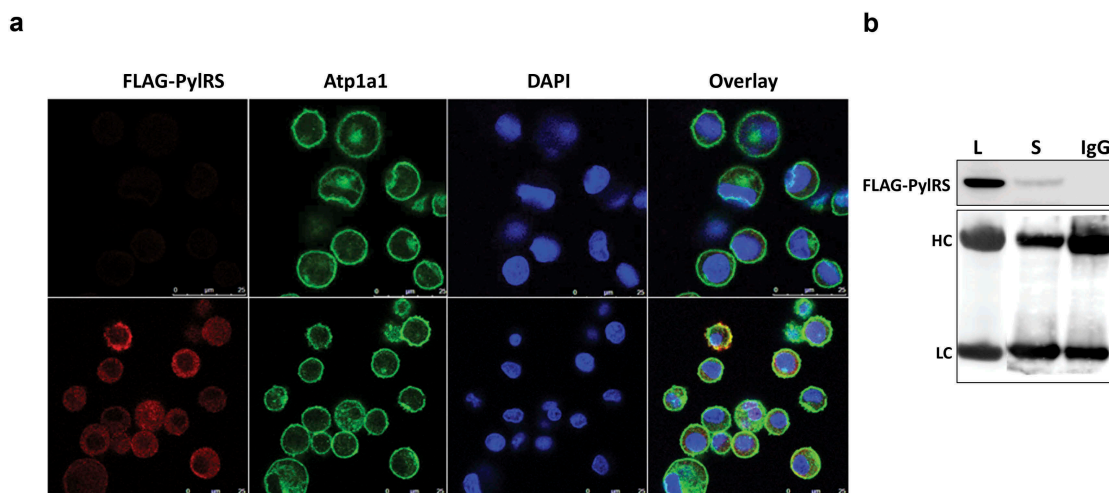
Figure 8. Intracellular localization of PylRS. (a) Localization of recombinant PylRS by confocal microscopy in primary isolates of IgG expressors in host 43 platform hosts. Cells were fixed and stained with anti-FLAG antibodies (PylRS) and the membrane protein Atp1p. DAPI was used to stain the nuclei. PylRS seems to localize to the cytoplasm of cells. **(b)** To examine whether PylRS is secreted, 50 μg of whole-cell lysates (L), 1 μg crude supernatants (S), and 1 ug of purified IgG derived from host 43 expressers were resolved by SDS-PAGE and examined by Western blotting. FLAG-tagged PylRS (upper panel) was detected using anti-FLAG antibody. IgG HC and LC were examined as loading controls (lower panel).

bioprocess or contaminates the final product. To begin to address this possibility, we first examined the subcellular distribution of PylRS by immunofluorescence confocal microscopy (Figure 8a). Antibody-expressing cells were fixed and stained for PylRS, a plasma membrane protein (Atp1a1) and nuclei (DAPI). We observed that PylRS co-localizes with the plasma membrane marker, but also shows cytoplasmic staining (Figure 8a). To assess whether PylRS is secreted and whether it co-purifies with IgG, we examined cell lysates (50 μg), cell supernatants (1 μg) and protein A purified IgG (1 μg) by Western blot analysis. PylRS was detected in cell supernatants of fed-batch cultures harvested on day 6, indicating that some of the expressed PylRS was escaping the cells. It is unclear whether the PylRS is secreted by the cells or is present in the supernatant as a result of cell lysis. It is notable that the cultures showed high viability at the time of sampling (98% viable), suggesting that the extracellular PylRS may not be entirely due to cell lysis. Nevertheless, PylRS was not detected in protein A-purified IgG (Figure 8b). These findings suggest that the potential for contamination of purified IgG product with PylRS protein is minimal, limiting the risk of immunogenicity.

Discussion

Methods for genetic code expansion are valuable strategies for introducing novel functionality into proteins. The most common way of introducing nnAAs is through stop codon suppression methods that require the function of orthogonal aaRS/tRNA pairs with specificity for a nnAA. This method has been shown to reliably deliver nnAAs to specific sites of a target protein. A variety of nnAAs with different functional moieties have been described that are useful for protein engineering, including altering protein structure and immunogenicity, stabilizing protein interactions, and mimicking post-translational modifications, but their most common application is to enable biorthogonal conjugations.[79] In particular, nnAA-based

conjugates have been shown to have superior stability as ADCs,[5] where the loss of payload in circulation adversely impacts both the safety and efficacy of drugs.[5,80,81] While these provide a significant improvement over conventional ADCs, low productivity of expression systems has limited their development. Indeed, few examples of high titer antibody expression are available.[15,18]

We developed a two-step screening strategy to identify a high-performance nnAA host platform. Cells were initially screened in a high throughput fashion with an amber suppression-dependent dual fluorescent mRNA reporter followed by screening for high titer IgGamb expression (Figure 2c). The fluorescent mRNA reporter was effective at identifying amber suppression competent cells (Figures 1a,b and Figure 2a,b), but, due to the limited dynamic range of fluorescence levels, it did not effectively discriminate cells with very high amber suppression activity. Thus, a secondary screen was implemented using an amber containing IgG to identify cells that were capable of high titer IgG expression.

Once the platform hosts capable of generating high titer, amber codon dependent expression were successfully identified, we characterized the hosts for the content of pylRS and tRNApyl. Using QPCR-based methods, we determined a correlation between IgGamb productivity and tRNApyl and PylRS copy number (Table 1).[76] Interestingly, in these cells gene copy number is a better indicator for IgGamb yield than tRNApyl and pylRS mRNA expression levels. Indeed, loss in IgG productivity due to phenotypic instability of the platform hosts can be correlated with reduced tRNApyl and PylRS gene copy numbers (Table 4). This is in contrast to conventional mAbs where mRNA levels correlate with titers. The trend may not apply to pylRS and tRNApyl levels because they function upstream of the gene of interest, creating a functional separation that provides an opportunity for regulation that we have yet to explain. Nevertheless, the copy number analysis is an important analytical metric to identify hosts with high amber suppression activity.

To establish the reproducibility of the host generation strategy, a second host cell line was developed using an engineered PylRS (Y306A) mutant capable of incorporating an expanded list of nnAAs. Interestingly, the PylRS bearing the Y306A mutation enables the incorporation of AzK, albeit with reduced efficiency, but also incorporates lysine analogues bearing cyclo- and spyrocyclopentadiene moieties (CpHK and SCpHK[27]). These latter nnAAs enable conjugation reactions in metal-free conditions with dienophiles (e.g., maleimide bearing molecules), allowing a rapid and effective formation of a stable linkage for next-generation ADCs.[78]

The manufacturability of this system was demonstrated by a reproducible, scalable manufacturing process based on perfusion technology that is suitable for both the WT and Y306A platform host-derived IgG-expressing cell lines for the incorporation of AzK, CpHK, and SCpHK nnAAs. These cells were shown to deliver a normalized titer ranging from 1.5 to 3.0 g/L, a reproducible yield that is acceptable for manufacturing. Interestingly, we observed that the cultures tolerated 40% amber suppression efficiency for 20–25 days (Figure 6a-d). A highly efficient amber suppression system in cell lines is necessary to support the expression demands required for the manufacturing of nnAA-containing therapeutic proteins. It should be noted that 25% of the CHO genome encodes proteins terminating with an amber stop codon (Baycin Hizal, unpublished data). While the amber codon is the least used of the stop codons in mammalian cells, it is expected that each of these codons will be suppressed in our host platform upon exposure to nnAA. We expect that global suppression of amber codons will result in the extension of essential cellular proteins that may alter their function and be deleterious to the cells, causing premature cell death and low IgG expression. Global amber codon suppression is mitigated in part by the strict orthogonality of the PylRS/tRNApyl pair and its specificity for nnAAs, which ensures that amber suppression occurs only in the presence of nnAA. If cytotoxicity did occur after the addition of nnAA due to amber suppression of cellular genes, the effects were not immediately observed. Rather, they were delayed 4–7 days, and even then, the loss of viability was relatively slow. The most affected culture was the one exposed to SCpHK that showed an early onset of loss of viability. This, however, is not likely due to amber suppression efficiency, as the SCpHK cells were no more efficient that the CpHK counterpart. The observe loss in viability may be due to cytotoxicity from the nnAA itself and requires additional characterization.

The platform cell lines described here have shown the ability to generate expression cell lines capable of high titer antibody expression in line with manufacturing requirements. However, the stability of the host platform is of critical importance to ensure consistent yields and product quality. In an effort to assess the general stability of the host cells, and the nnAA incorporation system, we opted to age a set of our platform hosts to 60 PDL prior to transfection and isolation of expression pools. Reduced nnAA IgG expression titers observed in platform hosts could be attributed to decreased cell viability and growth (host 43#8) or genetic instability of pylRS and tRNA genes (hosts 43, host 43#3, and host 43#37). In contrast, host Y306A36 retained pylRS/tRNA copy numbers and productivity over this passage number. These data

show that genetically stable hosts can be isolated despite the high number and repetitive nature of the gene constructs. However, to consider this as an expression system qualified for manufacturing, additional data on the stability of production cell lines as well as their product quality are needed.

The site of conjugation is an important consideration in the assembly of an ADC because it can affect the conjugation efficiency and potency of the drug. With the amber suppression technology, the site of the nnAA incorporation can also affect the expression yields. The materials generated by the perfusion process here were not selected for their expression potential, but rather for the functionality of the site. Indeed, we have observed productivity levels of 1.7 and 2 g/L in conventional fed-batch cultures with antibodies bearing nnAA at other sites. The sites selected for this study showed efficient conjugate formation with tubulysin containing either strain-promoted azide–alkyne cycloaddition (SPAAC) or maleimide chemistry (Figure 7a,b). Additionally, the conjugated material is highly potent and specific to target cells (Figure 7c). We also clearly demonstrated that, even though the archaebacterial PylRS is detected in the cell supernatants, it is not co-purified with secreted IgG products (Figure 8b). Co-expression of the bacterial PylRS in CHO cell lines for therapeutic mAb production is unlikely to pose a threat to patients by provoking immunogenicity to the PylRS protein.

Overall, these new cell lines provide a means for the production of ADCs with novel chemistries for conjugation and open opportunities for exploration of alternative sites of conjugation, not accessible to conventional chemistries, that may address current limitations observed with conventionally constructed ADCs. We show here that stable cell lines capable of genetically encoding nnAAs with high yields require high numbers and expression levels of the suppressor tRNApyl and its corresponding pylRS. Indeed, our best platforms demonstrate tRNApyl levels that are comparable in expression to 18S rRNA, a highly abundant message found in cells. The levels of pylRS are not in this vicinity, and may not be necessary, but a minimal level of expression is needed to effectively aminoacylate the available tRNApyl. Excess pylRS expression, however, has been shown to reduce nnAA incorporation efficiency.[69] Thus, a balance must be achieved that works cooperatively to potentiate amber suppression at high efficiency without creating unnecessary demands that affect viability and growth. Here we have relied on phenotypic selections to identify suitable host cells. However, further improvements to the efficacy of this expression system are necessary to increase the economy of producing nnAA-containing proteins, but also to enable the incorporation of multiple nnAAs, within a protein, for the construction of ADCs with high drug-to-antibody ratios. This may be achieved by implementing optimizations, such as the use of stabilized tRNApyl sequences,[65,70] overexpressing eRF1 mutations,[70] optimizing the expression levels of pylRS[72] and selecting optimal codon contexts for amber codons[63] that have been previously described in transient expression systems. These cell lines are not limited to the expression of antibodies and the generation of ADCs, but give access to any target protein that can be expressed in CHO cells. The functionality conveyed by the PylRS and tRNApyl pair may

also enable the construction of a novel, enhanced therapeutics for more effective treatment of human diseases.

Materials and methods

Transfection of CHO cells using plasmid DNA and synthetic mRNA and high throughput screening for amber suppression activity

Transfections were carried out with an Amaxa Nucleofector II device following the manufacturer's recommendations and using the Solution V kit (Lonza, Cat# VCA1003). For plasmid DNA transfections, 5×10^6 cells were transfected with 5.0 µg DNA prepared using an Endo-free plasmid Maxi kit (Qiagen, Cat# 12362). Synthetic mRNA encoding RFPamb-GFP (TriLink Biotechnologies) transfections were optimized using 1×10^6 cells and 1.7–3.4 pmol mRNA construct using program EH118 in a 96-well shuttle (Lonza). However, during high throughput screening, approximately 0.25×10^6 cells were transfected using 2.0 pmol synthetic mRNA to obtain optimal transfection efficiency. Nucleofected cells were recovered in 96-well plates containing CD-CHO medium (ThermoFisher Scientific, Cat# 10743029) supplemented with 6 mM L-glutamine (ThermoFisher Scientific Cat# 25030081). 2.0 mM AzK was used for inducing amber suppression activity. Functional screening of amber suppression activity by flow cytometry for detection of dual fluorescent (GFP- and RFP-positive cells) protein expression was carried out at 24-h post nucleofection using an LSRII cytometer (BD Biosciences) and data analyzed using FlowJo software (FLOWJO, LLC).

Generation of IgG-expressing stable pools for the screening of amber suppression positive hosts

CHO cells, derived from CHOK1, adapted to grow in suspension[73] were transfected using Amaxa 96-well shuttle (Lonza, Walkersville). For the generation of platform hosts, cells were transfected with a linearized plasmid encoding pylRS, 18 tandem repeats of the tRNApyl and a puromycin resistance cassette. Transfected cells were resuspended in CD-CHO medium containing 6.5 ug/ml puromycin, and cells plated into 96-well plates and incubated in a controlled environment incubator at 37°C with 6% CO₂. Wells showing colonies were harvested and expanded. Each colony was assessed for amber suppression activity using the RFPamb-GFP construct.[75,76] Colonies with the best GFP:RFP ratios were assessed for IgG expression. To do this, each colony was transfected with a linear mAb expression plasmid containing an amber codon at position 44 in HC and selected as mini pools in 24-well plates in CD-CHO medium supplemented with Puromycin (ThermoFisher Scientific, Cat# A1113802) and 50 µM methionine sulfoximine (MSX, Sigma-Aldrich, Cat# M5379). Surviving pools were expanded in shaking flasks. Amber suppression was induced in drug-selected mini-pools on day 4 of a 14-day fed-batch assay and IgG expression was monitored in 24 deep-well plates by biolayer interferometry using protein A-coated sensors. AstraZeneca-proprietary medium and feed were used for the fed-suspension assay.[73] Stable hosts were ranked based on IgG expression. Clonal hosts were generated by growing a host pool on semi-solid medium and colonies isolated using ClonePix FL. For the generation of stable IgG expresser colonies, platform hosts were nucleofected with a linearized plasmid encoding the IgG (containing an amber codon at the desired position), and a glutamine synthetase gene.[77] Transfected cells were plated into 96-well plates and grown in CD-CHO medium lacking glutamine and containing 50 µM MSX. Wells showing cell growth were selected and assessed for IgG expression in suspension growth conditions.

Genetic characterization of hosts by gene copy number and expression analyses of tRNApyl and PylRS by QPCR

Total RNA (tRNA, mRNA, and rRNA) was isolated from frozen cell pellets using the mirVANA miRNA Isolation kit (Ambion, Cat# AM1560) following the manufacturer's instructions. The purified RNA samples typically derived from a maximum of 5×10^6 cells were DNase treated using DNA-free kit (Ambion, Cat# AM1906). Genomic DNA (gDNA) was also isolated from a maximum of 5×10^6 cells kept as frozen pellets using the AllPrep DNA/RNA Mini Kit (Qiagen, Cat# 80204) by following the manufacturer's instructions. tRNApyl, PylRS, β2M mRNA expression levels were measured using TaqMan technology on the 7900HT Fast Real-Time PCR System (Life Technologies). The probes and primers were generated by assays-by-design (Applied Biosystems); the probes contain a 6-carboxy-fluoresceinphosphoramidite (FAM dye) label at the 5′end of the oligo and non-fluorescent (NFQ) or fluorescent quencher tetramethylrhodamine (TAMRA) at the 3′ end. qPCR was carried out by denaturing at 95°C for 20 s and then cycling at 95°C for 1 s and 60°C for 20 s, for 40 cycles. Primers for CHO-K1 β2M and 18S ribosomal RNA (18s) (Applied Biosystems, Cat# Hs99999901 s1) were used as the endogenous controls. Expression levels of tRNApyl processed and unprocessed and PylRS were normalized to endogenous CHO-K1 β2M or 18s. The sequence of the primers and probes are listed in Table 9.

Western blot analysis

Total IgG from crude cell supernatants was quantified using Protein A biosensors (Pall ForteBio Cat# 18–5013), 15 ng of which was resolved on SDS-PAGE (BioRad, Cat# 1656001)

Table 9. Primers and probes used for QPCR analyses.

Target gene	Primer type	Primer sequence
tRNApyl	Forward	5′- GGAAACCTGATCATGTAGATCG –3′
tRNApyl	Reverse	5′- GGAAACCCGGGAATC –3′
tRNApyl	Probe	5′-FAM- ACCCGGCTGAACGGATTTAGAGTC - TAMRA-3′
tRNApyl unprocessed	Forward	5′- GGAAACCTGATCATGTAGATCG –3′
tRNApyl unprocessed	Reverse	5′- CGCACTTGTCCGGAAAC –3′
tRNApyl unprocessed	Probe	5′-FAM- ACCCGGCTGAACGGATTTAGAGTC - TAMRA-3′
pylRSWT-Opt	Forward	5′- ATCAAGCACCATGAGGTGTC –3′
pylRSWT-Opt	Reverse	5′- ACCGCTTGCAGGTCTTTC –3′
pylRSWT-Opt	Probe	5′-FAM- GGGCCCAGCACGCTTCC -TAMRA-3′
CHO-K1 B2M	Forward	5′- CGAGCTGTTGAAGAATGGAAAGAAG –3′
CHO-K1 B2M	Reverse	5′- CGTGTGAGCCAAAAGATAGAAAGAC –3′
CHO-K1 B2M	Probe	5′-FAM- ACAAAGTCGAGCTGTCAGATCT-NFQ –3′

under non-reducing condition and transferred onto PVDF membrane (BioRad, Cat# 1620175) using a Trans-Blot Turbo transfer system (Bio-Rad, Cat# 1704150). Membranes were probed with horseradish peroxidase-conjugated goat anti-human IgG (Fab′)2 (Abcam Cat# ab87422) at 1:3000 dilution at room temperature for 1 h followed by 3-times washing in Tris-buffered saline (TBS) (Lonza, Cat# 1706435). Membranes were incubated briefly with Super-Signal West Pico Chemiluminescent Substrate (Thermo Scientific, Cat# 34078) followed by image analysis by ImageQuant LAS 4000 (GE Healthcare Bio-Sciences).

IgG purification

Full-length nnAA containing antibodies were captured from filtered cell culture supernatants by affinity chromatography (CaptureSelect FcXL, Life Technologies, Cat# 194328050). Bound IgG was washed with phosphate-buffered saline (PBS) pH 7.2 (Life Technologies, Cat# 20012050) and eluted with 0.1 M glycine pH 3.1 (Sigma, Cat# 410225) followed by neutralization with 20% v/v 1.0 M Tris pH 8.0 (Sigma, Cat# 93363). The purity of the IgG was confirmed by SDS-PAGE under reducing and non-reducing conditions and dialyzed to PBS pH 7.2 for long-term storage.

Octet-based assay for quantitation of full-length and total IgG

Full-length IgG quantitation was performed by bio-layer interferometry in the Octet RED96 System (PallForteBio). Streptavidin biosensors (PallForteBio, 18–5019) were soaked overnight at 4°C in mouse monoclonal H2 anti-human IgG Fc biotin (Abcam, ab99766) diluted to 5 μg/ml in PBS pH 7.2 (Thermo Fisher, 20012050). Excess unbound streptavidin was washed by equilibration of biosensors to the cell culture medium for 10 min at room temperature. Total IgG quantification was performed using Protein A biosensors (PallForteBio, Cat# 18–5013). Binding rate measurements were collected in the Octet device and quantified within the Octet software in reference to known concentrations of IgG standards.

Peptide mapping analysis

Antibody samples (100 μg) were denatured and reduced at 37°C for 30 min with buffer (1.3 M guanidine hydrochloride; 8 M urea; 130 mM Tris [tris (hydroxymethyl) amino-methane], pH 8.0; 6.5 mM dithiothreitol) followed by cooling at room temperature and alkylation by 2-iodoacetamide in the dark for 30 min. After alkylation, the samples were diluted 4 times (from 50 μL to 200 μL) with 100 mM Tris, pH 7.5, before digestion. Tryptic digests were performed at 37°C for 4 h and then quenched by the addition of 5 μL of 10% (vol/vol) trifluoroacetic acid (TFA). A Fusion Orbitrap mass spectro-meter (Thermo Fisher Scientific) connected with an AQUITY ultra-performance liquid chromatograph (UPLC; Waters) was used for peptide map analysis. An AQUITY UPLC BEH300 C18 column (1.7 μm, 2.1 × 150 mm; Waters) was used for separation. The column temperature was held at 55°C. Mobile

phase A was 0.02% TFA in water, and mobile phase B was 0.02% TFA in acetonitrile. Digested peptides were eluted from the column with a linear gradient of mobile phase B buffer from 5% to 40% B in 68.5 min then 40–95% B in 4.5 min and the chromatographic profile was monitored by using ultraviolet absorbance at 220 nm and mass spectrometry. Mass spectrometry data were processed by Biopharma Finder 2.0 (Thermo Fisher Scientific).

Intact-mass measurements

Intact-mass analysis was performed with a Waters SYNAPT G2-Si High Definition Mass Spectrometer in conjunction with a UPLC system (Waters). Purified antibody samples were diluted to 1 mg/mL in 100 mM Tris buffer at pH7.6 and deglycosylated using PNGase F at 37°C overnight. The degly-cosylated samples were desalted using reverse phase chroma-tography on a BEH C4 column (2.1 mm × 50 mm; Waters), using a mobile phase A composed of 0.1% formic acid (FA) and 0.01% TFA in water and a mobile phase B of 0.1% FA and 0.01% TFA in acetonitrile. Samples were eluted on a linear gradient from 5% to 80% B in 2 min, then 80% to 95% B in 2 min, and mass spectra were collected at m/z range of 800–4,500. Molecular mass was determined by deconvolution with the Maxent I software package (Waters, Milford, MA).

3L Perfusion bioreactors

Cells were cultured in 3 L stirred tank bioreactors using Eppendorf's DASGIP parallel bioreactor system. Bioreactors were inoculated from shake flask cultures to a working volume of 1.2 L and a starting cell density of 1.0×10^6 viable cells/mL using proprietary media. Operating parameters were monitored and controlled using DASware control software. Culture temperature, pH, and dissolved oxygen were maintained at 35.5°C, 7.00 ± 0.20, and 30%, respectively. The agitation was controlled at 350 rpm. Cell density and viability were measured using a Beckman Coulter Vi-CELL XR cell viability analyzer. Glucose, lactate, electrolytes, pH, pCO_2, and pO_2 were measured using a Siemens RAPIDPoint® 500 blood gas analyzer. Perfusion was initiated by alternating tangential flow filtration on day two of cultivation using proprie-tary enriched perfusion media. The culture was pumped back and forth through a Spectrum Labs Minikros Sampler hollow fiber module (P/N S04-P20U-10-N, polyethersulfone, 0.2 micron, 980 cm²). Repligen's XCell™ ATF C24 controller was used to control the recirculation rate at 0.4 L/min. Initial perfusion rate was set to five vessel volumes per day (VVD) and adjusted up to 4 VVD based on viable cell density measurements. nnAA was supplemented to the bioreactor culture and perfusion media on day 5 at a final concentration of 2 mM.

Azide-alkyne conjugation

Purified antibody containing AzK in PBS pH 7.2 (Life Technologies, 20012050) was incubated overnight with tubu-lysin-DBCO (eight-fold molar excess) at 20°C in the presence of 5 mM sodium phosphate monobasic (Sigma Catalog, Cat# S0751–100G) and 10% v/v dimethyl sulfoxide (Sigma Catalog, Cat# D1435–500 mL). Conjugated material was captured with

CHT II resin (BioRad, Cat# 158–2200) and washed promptly with 10 mM $NaPO_4$ pH 7.0 (Sigma, Cat# P2070). 2.0 M sodium chloride (J.T. Baker, Cat# 3624–19) was used to elute the conjugated mAb. Conjugation and purity were confirmed by SDS-PAGE and mass spectrometry.

Diels-Alder conjugation

Purified antibody containing CpK or SCpK in PBS pH 7.2 (Life Technologies, Cat# 20012050) was incubated for an hour with a maleimide-bearing payload (fivefold molar excess) at room temperature in presence of 10% $NaPO_4$ monobasic, pH 5.5 followed by quenching with four molar equivalents (relative to maleimide) of N-acetyl cysteine. Conjugated material was purified using CHT II resin (BioRad, Cat# 158–2200). Conjugation and purity were confirmed by SDS-PAGE and mass spectrometry.

Cytotoxicity assay

HER2-positive SK-BR-3 (ATCC, Cat# HTB-30), and HER2-negative MDA-MB-468 (ATCC, Cat# HTB-132) cells cultured in RPMI 1640 medium (Life Technologies, Cat# 20012050) supplemented with 10% fetal bovine serum were seeded at a density of 4,000 cells/well in 96-well white clear-bottom polystyrene microplates (Corning, Cat# 07–200–587) in 75 μL volume and allowed to grow overnight in humidified incubator at 37°C in presence of 5% CO_2. ADCs in PBS pH 7.2 (Life Technologies, Cat# 20012050) were serially diluted and added to each well with cells and incubated for 96 h. The viability of the treated cells was determined by adding CellTiter-Glo (Promega Corporation, Cat# G9242) and luminescence monitored using Perkin Elmer Envision Manager Software in Perkin Elmer Envision 2104 Multilabel Reader instrument. A non-linear regression model was used to fit the data for each sample and the half-maximal effective concentrations (EC50) calculated using GraphPad Prism software v8.

Localization of PylRS and confocal imaging

Actively growing cells were fixed in a freshly prepared 1:1 mixture of methanol and acetone for 1 min at room temperature followed by washing with 1xD-PBS (Invitrogen, Cat# 14190144) in a microfuge tube. The fixed cells were incubated at room temperature for an hour with 10 μg of APC-conjugated anti-FLAG M2 antibody (abcam, Cat# ab72569) in 100 μl of 3% BSA-PBS-T (Tween 0.1%) followed by an additional 30 min incubation with Alexa-488 labeled anti-alpha 1 sodium potassium ATPase antibody at 1:100 dilution (abcam Cat# ab197496). The excess antibodies were thoroughly washed with 1x PBS-T (Tween 0.1%). Stained cells were mounted on positively charged slides in presence of DAPI containing anti-fade mounting agent ProLong Gold Antifade Mountant (ThermoFisher, Cat# P36930), then visualized and imaged by confocal microscopy using a Leica SP5 (Leica Microsystems Inc.).

Abbreviations

ADC	antibody-drug conjugates
PylRS	pyrrolysyl-tRNA synthetase
IgG	immunoglobulin G
CHO	Chinese hamster ovary
nnAA	non-natural amino acids
tRNA	transfer ribo-nucleic acid

Disclosure of potential conflicts of interest

No potential conflicts of interests

ORCID

Gargi Roy http://orcid.org/0000-0002-8391-5067
Jason Reier http://orcid.org/0000-0003-1439-279X
Tom Martin http://orcid.org/0000-0002-7491-8274
Jihong Wang http://orcid.org/0000-0001-9271-0218
Meagan Prophet http://orcid.org/0000-0001-5518-3180
Sanjeev Ahuja http://orcid.org/0000-0002-2869-6885
Marcello Marelli http://orcid.org/0000-0001-7095-8263

References

1. Dall'Acqua WF, Kiener PA, Wu H. Properties of human IgG1s engineered for enhanced binding to the neonatal Fc receptor (FcRn). J Biol Chem. 2006;281:23514–24. doi:10.1074/jbc.M604292200.
2. Thakur A, Huang M, Lum LG. Bispecific antibody based therapeutics: strengths and challenges. Blood Rev. 2018;32:339–47. doi:10.1016/j.blre.2018.02.004.
3. Sliwkowski MX, Mellman I. Antibody therapeutics in cancer. Science. 2013;341:1192–98. doi:10.1126/science.1241145.
4. Zhu GD, Fu YX. Design of next generation antibody drug conjugates. Yao Xue Xue Bao. Acta Pharmaceutica Sinica. 2013;48:1053–70.
5. Hamblett KJ, Senter PD, Chace DF, Sun MM, Lenox J, Cerveny CG, Kissler KM, Bernhardt SX, Kopcha AK, Zabinski RF, et al. Effects of drug loading on the antitumor activity of a monoclonal antibody drug conjugate. Clin Can Res. 2004;10:7063–70. doi:10.1158/1078-0432.CCR-04-0789.
6. Junutula JR, Flagella KM, Graham RA, Parsons KL, Ha E, Raab H, Bhakta S, Nguyen T, Dugger DL, Li G, et al. Engineered thio-trastuzumab-DM1 conjugate with an improved therapeutic index to target human epidermal growth factor receptor 2-positive breast cancer. Clin Can Res. 2010;16:4769–78. doi:10.1158/1078-0432.CCR-10-0987.
7. Bender B, Leipold DD, Xu K, Shen BQ, Tibbitts J, Friberg LE. A mechanistic pharmacokinetic model elucidating the disposition of trastuzumab emtansine (T-DM1), an antibody-drug conjugate (ADC) for treatment of metastatic breast cancer. Aaps J. 2014;16:994–1008. doi:10.1208/s12248-014-9618-3.
8. Jeffrey SC, Burke PJ, Lyon RP, Meyer DW, Sussman D, Anderson M, Hunter JH, Leiske CI, Miyamoto JB, Nicholas ND, et al. A potent anti-CD70 antibody-drug conjugate combining a dimeric pyrrolo-benzodiazepine drug with site-specific conjugation technology. Bioconjug Chem. 2013;24:1256–63. doi:10.1021/bc400217g.
9. Dimasi N, Fleming R, Zhong H, Bezabeh B, Kinneer K, Christie RJ, Fazenbaker C, Wu H, Gao C. Efficient preparation of site-specific antibody-drug conjugates using cysteine insertion. Mol Pharm. 2017;14:1501–16. doi:10.1021/acs.molpharmaceut.6b00995.
10. Shen BQ, Xu K, Liu L, Raab H, Bhakta S, Kenrick M, Parsons-Reponte KL, Tien J, Yu S-F, Mai E, et al. Conjugation site

modulates the in vivo stability and therapeutic activity of antibody-drug conjugates. Nat Biotechnol. 2012;30:184–89. doi:10.1038/nbt.2108.

11. Agarwal P, Bertozzi CR. Site-specific antibody-drug conjugates: the nexus of bioorthogonal chemistry, protein engineering, and drug development. Bioconjug Chem. 2015;26:176–92. doi:10.1021/bc5004982.

12. Boutureira O, Bernardes GJ. Advances in chemical protein modification. Chem Rev. 2015;115:2174–95. doi:10.1021/cr500399p.

13. Nguyen DP, Lusic H, Neumann H, Kapadnis PB, Deiters A, Chin JW. Genetic encoding and labeling of aliphatic azides and alkynes in recombinant proteins via a pyrrolysyl-tRNA Synthetase/tRNA(CUA) pair and click chemistry. J Am Chem Soc. 2009;131:8720–21. doi:10.1021/ja900553w.

14. Axup JY, Bajjuri KM, Ritland M, Hutchins BM, Kim CH, Kazane SA, Halder R, Forsyth JS, Santidrian AF, Stafin K, et al. Synthesis of site-specific antibody-drug conjugates using unnatural amino acids. Proc Natl Acad Sci USA. 2012;109:16101–06. doi:10.1073/pnas.1211023109.

15. Tian F, Lu Y, Manibusan A, Sellers A, Tran H, Sun Y, Phuong T, Barnett R, Hehli B, Song F, et al. A general approach to site-specific antibody drug conjugates. Proc Natl Acad Sci USA. 2014;111:1766–71.

16. Zimmerman ES, Heibeck TH, Gill A, Li X, Murray CJ, Madlansacay MR, Tran C, Uter NT, Yin G, Rivers PJ, et al. Production of site-specific antibody-drug conjugates using optimized non-natural amino acids in a cell-free expression system. Bioconjug Chem. 2014;25:351–61. doi:10.1021/bc400490z.

17. Jackson D, Atkinson J, Guevara CI, Zhang C, Kery V, Moon SJ, Virata C, Yang P, Lowe C, Pinkstaff J, et al. In vitro and in vivo evaluation of cysteine and site specific conjugated herceptin antibody-drug conjugates. PLoS One. 2014;9:e83865. doi:10.1371/journal.pone.0083865.

18. VanBrunt MP, Shanebeck K, Caldwell Z, Johnson J, Thompson P, Martin T, Dong H, Li G, Xu H, D'Hooge F, et al. Genetically encoded azide containing amino acid in mammalian cells enables site-specific antibody-drug conjugates using click cycloaddition chemistry. Bioconjug Chem. 2015;26:2249–60. doi:10.1021/acs.bioconjchem.5b00359.

19. Thompson P, Ezeadi E, Hutchinson I, Fleming R, Bezabeh B, Lin J, Mao S, Chen C, Masterson L, Zhong H, et al. Straightforward glycoengineering approach to site-specific antibody-pyrrolobenzodiazepine conjugates. ACS Med Chem Lett. 2016;7:1005–08. doi:10.1021/acsmedchemlett.6b00278.

20. Barfield RM, Rabuka D. Leveraging formylglycine-generating enzyme for production of site-specifically modified bioconjugates. Methods Mol Biol. 2018;1728:3–16.

21. Okeley NM, Toki BE, Zhang X, Jeffrey SC, Burke PJ, Alley SC, Senter PD. Metabolic engineering of monoclonal antibody carbohydrates for antibody-drug conjugation. Bioconjug Chem. 2013;24:1650–55. doi:10.1021/bc4002695.

22. Zhou Q, JE S, Manning C, Kyazike J, Chen B, DA G, Park A, Busch M, Bird J, Zheng X, et al. Site-specific antibody-drug conjugation through glycoengineering. Bioconjug Chem. 2014;25:510–20. doi:10.1021/bc400505q.

23. Verkade JMM, Wijdeven MA, Van Geel R, Janssen BMG, Van Berkel SS, Van Delft FL. A polar sulfamide spacer significantly enhances the manufacturability, stability, and therapeutic index of antibody–drug conjugates. Antibodies. 2018;7:12.

24. Chin JW. Expanding and reprogramming the genetic code of cells and animals. Annu Rev Biochem. 2014;83:379–408. doi:10.1146/annurev-biochem-060713-035737.

25. Chin JW. Expanding and reprogramming the genetic code. Nature. 2017;550:53–60. doi:10.1038/nature24031.

26. Tsuchikama K, An Z. Antibody-drug conjugates: recent advances in conjugation and linker chemistries. Protein Cell. 2018;9:33–46. doi:10.1007/s13238-016-0323-0.

27. St Amant AH, Huang F, Lin J, Rickert K, Oganesyan V, Lemen D, Mao S, Harper J, Marelli M, Wu H, et al. A diene-containing noncanonical amino acid enables dual functionality in proteins:

rapid diels-alder reaction with maleimide or proximity-based dimerization. Angew Chem. 2019;58:8489–93. doi:10.1002/anie.201903494.

28. Kiick KL, Saxon E, Tirrell DA, Bertozzi CR. Incorporation of azides into recombinant proteins for chemoselective modification by the Staudinger ligation. Proc Natl Acad Sci. 2002;99:19–24. doi:10.1073/pnas.012583299.

29. Chin JW, Santoro SW, Martin AB, King DS, Wang L, Schultz PG. Addition of p-azido-L-phenylalanine to the genetic code of Escherichia coli. J Am Chem Soc. 2002;124:9026–27. doi:10.1021/ja027007w.

30. Lang K, Davis L, Wallace S, Mahesh M, Cox DJ, Blackman ML, Fox JM, Chin JW. Genetic encoding of bicyclononynes and trans-cyclooctenes for site-specific protein labeling in vitro and in live mammalian cells via rapid fluorogenic diels-alder reactions. J Am Chem Soc. 2012;134:10317–20. doi:10.1021/ja302832g.

31. Neumann H, Hancock SM, Buning R, Routh A, Chapman L, Somers J, Owen-Hughes T, van Noort J, Rhodes D, Chin JW, et al. A method for genetically installing site-specific acetylation in recombinant histones defines the effects of H3 K56 acetylation. Mol Cell. 2009;36:153–63. doi:10.1016/j.molcel.2009.07.027.

32. Neumann H, Peak-Chew SY, Chin JW. Genetically encoding N(epsilon)-acetyllysine in recombinant proteins. Nat Chem Biol. 2008;4:232–34. doi:10.1038/nchembio.73.

33. Wilkins BJ, Rall NA, Ostwal Y, Kruitwagen T, Hiragami-Hamada K, Winkler M, Barral Y, Fischle W, Neumann H. A cascade of histone modifications induces chromatin condensation in mitosis. Science. 2014;343:77–80. doi:10.1126/science.1244508.

34. Brustad EM, Lemke EA, Schultz PG, Deniz AA. A general and efficient method for the site-specific dual-labeling of proteins for single molecule fluorescence resonance energy transfer. J Am Chem Soc. 2008;130:17664–65. doi:10.1021/ja807430h.

35. Miyake-Stoner SJ, Miller AM, Hammill JT, Peeler JC, Hess KR, Mehl RA, Brewer SH. Probing protein folding using site-specifically encoded unnatural amino acids as FRET donors with tryptophan. Biochemistry. 2009;48:5953–62. doi:10.1021/bi900426d.

36. Kalstrup T, Blunck R. Dynamics of internal pore opening in K(V) channels probed by a fluorescent unnatural amino acid. Proc Natl Acad Sci USA. 2013;110:8272–77. doi:10.1073/pnas.1220398110.

37. Milles S, Lemke EA. Single molecule study of the intrinsically disordered FG-repeat nucleoporin 153. Biophys J. 2011;101:1710–19. doi:10.1016/j.bpj.2011.08.025.

38. Kwon I, Tirrell DA. Site-specific incorporation of tryptophan analogues into recombinant proteins in bacterial cells. J Am Chem Soc. 2007;129:10431–37. doi:10.1021/ja071773r.

39. Wang K, Neumann H, Peak-Chew SY, Chin JW. Evolved orthogonal ribosomes enhance the efficiency of synthetic genetic code expansion. Nat Biotechnol. 2007;25:770–77. doi:10.1038/nbt1314.

40. Tropberger P, Pott S, Keller C, Kamieniarz-Gdula K, Caron M, Richter F, Li G, Mittler G, Liu E, Bühler M, et al. Regulation of transcription through acetylation of H3K122 on the lateral surface of the histone octamer. Cell. 2013;152:859–72. doi:10.1016/j.cell.2013.01.032.

41. Okuda S, Freinkman E, Kahne D. Cytoplasmic ATP hydrolysis powers transport of lipopolysaccharide across the periplasm in E. coli. Science. 2012;338:1214–17. doi:10.1126/science.1228984.

42. Tang Y, Ghirlanda G, Vaidehi N, Kua J, Mainz DT, Goddard IW, DeGrado WF, Tirrell DA. Stabilization of coiled-coil peptide domains by introduction of trifluoroleucine. Biochemistry. 2001;40:2790–96. doi:10.1021/bi0022588.

43. Wang L, Brock A, Herberich B, Schultz PG. Expanding the genetic code of Escherichia coli. Science. 2001;292:498–500. doi:10.1126/science.1060077.

44. Kwon I, Wang P, Tirrell DA. Design of a bacterial host for site-specific incorporation of p-bromophenylalanine into recombinant proteins. J Am Chem Soc. 2006;128:11778–83. doi:10.1021/ja0626281.

45. Italia JS, Addy PS, Wrobel CJ, Crawford LA, Lajoie MJ, Zheng Y, Chatterjee A. An orthogonalized platform for genetic code expansion in both bacteria and eukaryotes. Nat Chem Biol. 2017;13:446–50. doi:10.1038/nchembio.2312.

46. Chin JW, Cropp TA, Anderson JC, Mukherji M, Zhang Z, Schultz PG. An expanded eukaryotic genetic code. Science. 2003;301:964–67. doi:10.1126/science.1084772.

47. Chin JW, Cropp TA, Chu S, Meggers E, Schultz PG. Progress toward an expanded eukaryotic genetic code. Chem Biol. 2003;10:511–19. doi:10.1016/S1074-5521(03)00123-6.

48. Edwards H, Schimmel P. A bacterial amber suppressor in Saccharomyces cerevisiae is selectively recognized by a bacterial aminoacyl-tRNA synthetase. Mol Cell Biol. 1990;10:1633–41. doi:10.1128/MCB.10.4.1633.

49. Edwards H, Trezeguet V, Schimmel P. An Escherichia coli tyrosine transfer RNA is a leucine-specific transfer RNA in the yeast Saccharomyces cerevisiae. Proc Natl Acad Sci USA. 1991;88:1153–56. doi:10.1073/pnas.88.4.1153.

50. Trezeguet V, Edwards H, Schimmel P. A single base pair dominates over the novel identity of an Escherichia coli tyrosine tRNA in Saccharomyces cerevisiae. Mol Cell Biol. 1991;11:2744–51. doi:10.1128/MCB.11.5.2744.

51. Sakamoto K, Hayashi A, Sakamoto A, Kiga D, Nakayama H, Soma A, Kobayashi T, Kitabatake M, Takio K, Saito K, et al. Site-specific incorporation of an unnatural amino acid into proteins in mammalian cells. Nucleic Acids Res. 2002;30:4692–99. doi:10.1093/nar/gkf589.

52. Liu W, Brock A, Chen S, Chen S, Schultz PG. Genetic incorporation of unnatural amino acids into proteins in mammalian cells. Nat Methods. 2007;4:239–44. doi:10.1038/nmeth1016.

53. Hancock SM, Uprety R, Deiters A, Chin JW. Expanding the genetic code of yeast for incorporation of diverse unnatural amino acids via a pyrrolysyl-tRNA synthetase/tRNA pair. J Am Chem Soc. 2010;132:14819–24. doi:10.1021/ja104609m.

54. Mukai T, Kobayashi T, Hino N, Yanagisawa T, Sakamoto K, Yokoyama S. Adding l-lysine derivatives to the genetic code of mammalian cells with engineered pyrrolysyl-tRNA synthetases. Biochem Biophys Res Commun. 2008;371:818–22. doi:10.1016/j.bbrc.2008.04.164.

55. Chen PR, Groff D, Guo J, Ou W, Cellitti S, Geierstanger BH, Schultz PG. A facile system for encoding unnatural amino acids in mammalian cells. Angew Chem. 2009;48:4052–55. doi:10.1002/anie.200900683.

56. Gautier A, Nguyen DP, Lusic H, An W, Deiters A, Chin JW. Genetically encoded photocontrol of protein localization in mammalian cells. J Am Chem Soc. 2010;132:4086–88. doi:10.1021/ja910688s.

57. Greiss S, Chin JW. Expanding the genetic code of an animal. J Am Chem Soc. 2011;133:14196–99. doi:10.1021/ja2054034.

58. Bianco A, Townsley FM, Greiss S, Lang K, Chin JW. Expanding the genetic code of Drosophila melanogaster. Nat Chem Biol. 2012;8:748–50. doi:10.1038/nchembio.1043.

59. Bertram G, Innes S, Minella O, Richardson J, Stansfield I. Endless possibilities: translation termination and stop codon recognition. Microbiology. 2001;147:255–69. doi:10.1099/00221287-147-2-255.

60. Cridge AG, Crowe-McAuliffe C, Mathew SF, Tate WP. Eukaryotic translational termination efficiency is influenced by the 3′ nucleotides within the ribosomal mRNA channel. Nucleic Acids Res. 2018;46:1927–44. doi:10.1093/nar/gkx1315.

61. Diago-Navarro E, Mora L, Buckingham RH, Diaz-Orejas R, Lemonnier M. Novel Escherichia coli RF1 mutants with decreased translation termination activity and increased sensitivity to the cytotoxic effect of the bacterial toxins Kid and RelE. Mol Microbiol. 2009;71:66–78. doi:10.1111/mmi.2009.71.issue-1.

62. Wilusz JE. Controlling translation via modulation of tRNA levels. Wiley Interdiscip Rev RNA. 2015;6:453–70. doi:10.1002/wrna.1287.

63. Pott M, Schmidt MJ, Summerer D. Evolved sequence contexts for highly efficient amber suppression with noncanonical amino acids. ACS Chem Biol. 2014;9:2815–22. doi:10.1021/cb5006273.

64. Guo J, Melancon CE 3rd, Lee HS, Groff D, Schultz PG. Evolution of amber suppressor tRNAs for efficient bacterial production of proteins containing nonnatural amino acids. Angew Chem. 2009;48:9148–51. doi:10.1002/anie.200904035.

65. Serfling R, Lorenz C, Etzel M, Schicht G, Bottke T, Morl M, Coin I. Designer tRNAs for efficient incorporation of non-canonical amino acids by the pyrrolysine system in mammalian cells. Nucleic Acids Res. 2018;46:1–10. doi:10.1093/nar/gkx1156.

66. Chatterjee A, Sun SB, Furman JL, Xiao H, Schultz PG. A versatile platform for single- and multiple-unnatural amino acid mutagenesis in Escherichia coli. Biochemistry. 2013;52:1828–37. doi:10.1021/bi4000244.

67. Zhang Y, Ptacin JL, Fischer EC, Aerni HR, Caffaro CE, San Jose K, Feldman AW, Turner CR, Romesberg FE. A semi-synthetic organism that stores and retrieves increased genetic information. Nature. 2017;551:644–47. doi:10.1038/nature24659.

68. Dalton AC, Barton WA. Over-expression of secreted proteins from mammalian cell lines. Protein Sci. 2014;23:517–25. doi:10.1002/pro.2439.

69. Zheng Y, Lewis TL Jr., Igo P, Polleux F, Chatterjee A. Virus-enabled optimization and delivery of the genetic machinery for efficient unnatural amino acid mutagenesis in mammalian cells and tissues. ACS Synth Biol. 2017;6:13–18. doi:10.1021/acssynbio.6b00092.

70. Schmied WH, Elsasser SJ, Uttamapinant C, Chin JW. Efficient multisite unnatural amino acid incorporation in mammalian cells via optimized pyrrolysyl tRNA synthetase/tRNA expression and engineered eRF1. J Am Chem Soc. 2014;136:15577–83. doi:10.1021/ja5069728.

71. Xiang L, Moncivais K, Jiang F, Willams B, Alfonta L, Zhang ZJ. Crucial optimization of translational components towards efficient incorporation of unnatural amino acids into proteins in mammalian cells. PLoS One. 2013;8:e67333. doi:10.1371/journal.pone.0067333.

72. Chatterjee A, Xiao H, Bollong M, Ai HW, Schultz PG. Efficient viral delivery system for unnatural amino acid mutagenesis in mammalian cells. Proc Natl Acad Sci USA. 2013;110:11803–08. doi:10.1073/pnas.1309584110.

73. Roy G, Zhang S, Li L, Higham E, Wu H, Marelli M, Bowen MA. Development of a fluorescent reporter system for monitoring ER stress in Chinese hamster ovary cells and its application for therapeutic protein production. PLoS One. 2017;12:e0183694. doi:10.1371/journal.pone.0183694.

74. Roy G, Martin T, Barnes A, Wang J, Jimenez RB, Rice M, Li L, Feng H, Zhang S, Chaerkady R, et al. A novel bicistronic gene design couples stable cell line selection with a fucose switch in a designer CHO host to produce native and afucosylated glycoform antibodies. MAbs. 2018;10:416–30. doi:10.1080/19420862.2018.1433975.

75. Chakrabarti L, Zhuang L, Roy G, Bowen MA, Dall'Acqua WF, Hawley-Nelson P, Marelli M. Amber suppression coupled with inducible surface display identifies cells with high recombinant protein productivity. Biotechnol Bioeng. 2019;116:793–804. doi:10.1002/bit.26892.

76. Garcia A, Roy G, Kiefer C, Wilson S, Marelli M. qPCR assays to quantitate tRNApyl and pylRS expression in engineered cell lines. PLoS One. 2019;14:e0216356. doi:10.1371/journal.pone.0216356.

77. Roy G, Miro-Quesada G, Zhuang L, Martin T, Zhu J, Wu H, Marelli M, Bowen MA. Sequential screening by ClonePix FL and intracellular staining facilitate isolation of high producer cell lines for monoclonal antibody manufacturing. J Immunol Methods. 2017;451:100–10. doi:10.1016/j.jim.2017.08.012.

78. St Amant AH, Lemen D, Florinas S, Mao S, Fazenbaker C, Zhong H, Wu H, Gao C, Christie RJ, Read de Alaniz J, et al. Tuning the diels-alder reaction for bioconjugation to maleimide drug-linkers. Bioconjug Chem. 2018;29:2406–14. doi:10.1021/acs.bioconjchem.8b00320.

79. Neumann H. Rewiring translation - Genetic code expansion and its applications. FEBS Lett. 2012;586:2057–64. doi:10.1016/j.febslet.2012.02.002.

80. Jackson DY. Processes for constructing homogeneous antibody-drug conjugates. Org Process Res Dev. 2016;20:852–66. doi:10.1021/acs.oprd.6b00067.

81. Krop IE, Beeram M, Modi S, Jones SF, Holden SN, Yu W, Girish S, Tibbitts J, Yi J-H, Sliwkowski MX, et al. Phase I study of trastuzumab-DM1, an HER2 antibody-drug conjugate, given every 3 weeks to patients with HER2-positive metastatic breast cancer. J Clin Oncol. 2010;28:2698–704. doi:10.1200/JCO.2009.26.2071.